



This is a repository copy of *Boosting the osteogenic and angiogenic performance of multiscale porous polycaprolactone scaffolds by In vitro generated extracellular matrix decoration.*

White Rose Research Online URL for this paper:  
<http://eprints.whiterose.ac.uk/158779/>

Version: Published Version

---

**Article:**

Aldemir Dikici, B. [orcid.org/0000-0002-5516-469X](https://orcid.org/0000-0002-5516-469X), Reilly, G.C. [orcid.org/0000-0003-1456-1071](https://orcid.org/0000-0003-1456-1071) and Claeysens, F. [orcid.org/0000-0002-1030-939X](https://orcid.org/0000-0002-1030-939X) (2020) Boosting the osteogenic and angiogenic performance of multiscale porous polycaprolactone scaffolds by In vitro generated extracellular matrix decoration. *ACS Applied Materials & Interfaces*, 12 (11). pp. 12510-12524. ISSN 1944-8244

<https://doi.org/10.1021/acsami.9b23100>

---

**Reuse**

This article is distributed under the terms of the Creative Commons Attribution (CC BY) licence. This licence allows you to distribute, remix, tweak, and build upon the work, even commercially, as long as you credit the authors for the original work. More information and the full terms of the licence here:  
<https://creativecommons.org/licenses/>

**Takedown**

If you consider content in White Rose Research Online to be in breach of UK law, please notify us by emailing [eprints@whiterose.ac.uk](mailto:eprints@whiterose.ac.uk) including the URL of the record and the reason for the withdrawal request.



[eprints@whiterose.ac.uk](mailto:eprints@whiterose.ac.uk)  
<https://eprints.whiterose.ac.uk/>

# Boosting the Osteogenic and Angiogenic Performance of Multiscale Porous Polycaprolactone Scaffolds by *In Vitro* Generated Extracellular Matrix Decoration

Betül Aldemir Dikici, Gwendolen C. Reilly, and Frederik Claeyssens\*

Cite This: *ACS Appl. Mater. Interfaces* 2020, 12, 12510–12524

Read Online

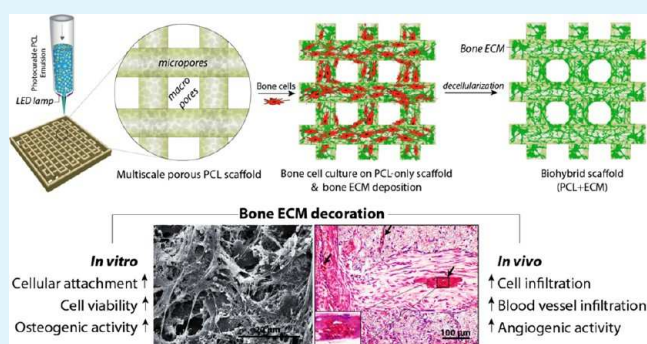
ACCESS |

Metrics & More

Article Recommendations

**ABSTRACT:** Tissue engineering (TE)-based bone grafts are favorable alternatives to autografts and allografts. Both biochemical properties and the architectural features of TE scaffolds are crucial in their design process. Synthetic polymers are attractive biomaterials to be used in the manufacturing of TE scaffolds, due to various advantages, such as being relatively inexpensive, enabling precise reproducibility, possessing tunable mechanical/chemical properties, and ease of processing. However, such scaffolds need modifications to improve their limited interaction with biological tissues. Structurally, multiscale porosity is advantageous over single-scale porosity; therefore, in this study, we have considered two key points in the design of a bone repair material; (i) manufacture of multiscale porous scaffolds made of photocurable polycaprolactone (PCL) by a combination of emulsion templating and three-dimensional (3D) printing and (ii) decoration of these scaffolds with the *in vitro* generated bone-like extracellular matrix (ECM) to create biohybrid scaffolds that have improved biological performance compared to PCL-only scaffolds. Multiscale porous scaffolds were fabricated, bone cells were cultured on them, and then they were decellularized. The biological performance of these constructs was tested *in vitro* and *in vivo*. Mesenchymal progenitors were seeded on PCL-only and biohybrid scaffolds. Cells not only showed improved attachment on biohybrid scaffolds but also exhibited a significantly higher rate of cell growth and osteogenic activity. The chick chorioallantoic membrane (CAM) assay was used to explore the angiogenic potential of the biohybrid scaffolds. The CAM assay indicated that the presence of the *in vitro* generated ECM on polymeric scaffolds resulted in higher angiogenic potential and a high degree of tissue infiltration. This study demonstrated that multiscale porous biohybrid scaffolds present a promising approach to improve bioactivity, encourage precursors to differentiate into mature bones, and to induce angiogenesis.

**KEYWORDS:** tissue engineering, emulsion templating, 3D printing, decellularization, angiogenesis, polyHIPE, biohybrid



## 1. INTRODUCTION

Bone grafting is the second most frequent tissue transplantation technique worldwide after blood transfusion.<sup>1</sup> Autogenous bone grafts are considered to be the gold standard as they have osteogenic, osteoinductive, and osteoconductive properties.<sup>2–4</sup> However, the autologous bone is mostly harvested from the iliac crest (hip) with limited availability and carries the risk of donor site morbidity.<sup>5</sup> An acellular alternative to the autograft is an allograft, which is more abundantly available without size limitations.<sup>6</sup> However, allografts need to be processed and cleaned after isolation to prevent an immune response and disease transmission.<sup>7,8</sup> These treatments considerably affect the physical and biological properties of the bone, and the process results in grafts with comparably poor regenerative potential and/or weak mechanical properties depending on the treatment (demineralization, deproteination, and irradiation).<sup>2,7</sup> The regulations of

the European Union for medical devices, known as the Medical Device Directive (MDD),<sup>9</sup> were replaced with a new set of Medical Device Regulations (MDR)<sup>10</sup> in 2017, and the new MDR will come into force on May 2020. With the new MDR, human origin cells and tissues or derivatives will also be considered as a high-risk medical device (class III) in addition to those of animal origin (rule 18). Due to these regulatory restrictions, allografts including demineralized and deproteinized bone (DMB and DPB) matrices will likely have more

Received: December 21, 2019

Accepted: February 26, 2020

Published: February 26, 2020

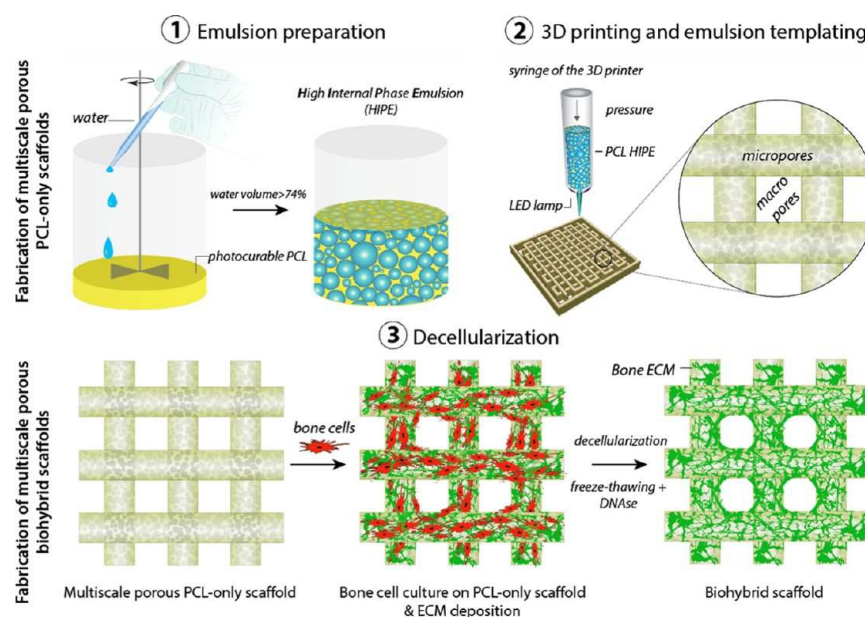


**Figure 1.** Manufacturing routes of the multiscale porous photocurable polycaprolactone (PCL) scaffolds (steps 1, 2) and multiscale porous biohybrid scaffolds (steps 1–3). (1) Preparation of the emulsion made of photocurable PCL and water, (2) the transfer of the PCL-based high internal phase emulsion (HIPE) into the syringe, pressure-assisted 3D printing, and simultaneous cross-linking, and (3) the culture of bone cells on the PCL-only scaffold to be decellularized and generation of the biohybrid scaffolds.

restrictive approval processes and a more challenging pathway for clinical approval.<sup>11–13</sup>

Alternatively, scaffold-based tissue engineering (TE) has gained great attention over the last years. Scaffolds are biodegradable porous matrices, made from natural or synthetic materials, which aim to mimic both the biochemical and structural features of native tissues for the regeneration of the defect site.<sup>14–16</sup>

To date, several techniques, including electrospinning,<sup>17,18</sup> particle leaching,<sup>19,20</sup> freeze-drying,<sup>21,22</sup> and additive manufacturing,<sup>23,24</sup> have been widely used for fabrication of bone TE scaffolds. Recently, emulsion templating has gained particular attention as a scaffold fabrication technique due to its ability to introduce up to 99% porosity with high interconnectivity into TE scaffolds. Emulsion templating is based on creating a stable emulsion by mixing two immiscible liquids and then polymerizing the continuous phase. Emulsion droplets act as a pore template during polymerization, and they are removed afterward. When the internal phase volume (total droplet volume) of the emulsion is greater than 74%, it is defined as a high internal phase emulsion (HIPE). Typically, the average pore range of polymerized HIPEs (polyHIPEs) varies from microns to tens of microns.<sup>25</sup> As multiple length scale porosity is advantageous for bone regeneration when compared to single-scale porosity,<sup>26</sup> combining emulsion templating with additive manufacturing enables the fabrication of hierarchically porous scaffolds.<sup>27–30</sup>

PolyHIPEs are most commonly created using water-in-oil (w/o) emulsions where a synthetic hydrophobic polymer is used as the continuous phase. Synthetic polymers have various advantages over ceramics and natural polymers, such as having tailorable physical, chemical, and mechanical properties, precise reproducibility, controllable biodegradability, and processability.<sup>31–33</sup> However, they have the disadvantage of having comparably limited interaction with biological tissues.<sup>34,35</sup> One approach to overcome this limitation is the decoration of polymeric scaffolds with ceramic particles<sup>36</sup> or

exogenous extracellular matrix (ECM) components,<sup>37</sup> such as peptides,<sup>38,39</sup> proteins, and growth factors.<sup>40,41</sup> Nevertheless, the incorporation of a limited number of exogenous ECM elements is not entirely sufficient to mimic the unique complexity of the natural ECM,<sup>42</sup> which is a rich source of bioactive molecules.<sup>43,44</sup> For this reason, TE adopts cell-based approaches in which live cells are implanted with the biomaterial. However, the use of live cells is clinically risky, expensive, and time consuming.<sup>45</sup> Therefore, there has been an increasing interest in using a cell-derived ECM to increase the biological performance of the scaffolds while avoiding the implantation of live cells.<sup>2,44,46–50</sup>

Recently, we reported the development of polycaprolactone (PCL)-based polyHIPEs and demonstrated their initial cell compatibility<sup>51</sup> and their potential use in guided bone regeneration.<sup>52</sup> However, due to the hydrophobic nature of the PCL, cell infiltration was limited unless the PCL-based scaffolds were treated with air plasma.<sup>52</sup> Although there is an increasing demand for the use of emulsion-templated scaffolds for various TE applications<sup>53,54</sup> due to their ability to create structures with favorable morphological properties, there are only a limited number of studies establishing methods to improve the cell–material interactions of polyHIPE scaffolds, and these are limited to the incorporation of a single biologically active agent<sup>55,56</sup> or hydroxyapatite (HA).<sup>57,58</sup>

Herein, we aimed to consider both the structural and biochemical requirements for the development of scaffolds for bone regeneration and suggest an alternative approach to improve the biological performance of w/o polyHIPEs. First, we manufactured multiscale porous polymeric scaffolds by combining emulsion templating and three-dimensional (3D) printing techniques, taking advantage of the photocure ability of the synthesized PCL (Figure 1). Subsequently, we populated them with bone cells to decorate these scaffolds with an *in vitro* cell-derived ECM. Finally, we decellularized these constructs to obtain biohybrid scaffolds made of PCL and the bone-like matrix. The biohybrid scaffolds were then

evaluated for their ability to support cell attachment, cell viability, and osteogenic differentiation using human embryonic stem cell-derived mesenchymal progenitor cells (hES-MPs). The angiogenic potential of the biohybrid multiscale porous scaffolds was assessed using a well-established *in vivo* assay, an *ex ovo* chick chorioallantoic membrane assay (CAM).

## 2. EXPERIMENTAL SECTION

**2.1. Materials.** Pentaerythritol (98%),  $\epsilon$ -caprolactone, tin(II) 2-ethyl hexanoate, triethylamine (TEA), methacrylic anhydride (MAAn), photoinitiator (2,4,6-trimethyl benzoyl phosphine oxide/2-hydroxy-2-methylpropiophenone blend), fetal calf serum (FCS), penicillin/streptomycin, L-glutamine, trypsin, 37% formaldehyde (FA) solution, resazurin sodium salt, glutaraldehyde, ethanol, hydrochloric acid (HCl), sodium hydroxide (NaOH), hexamethyldisilazane (HMDS), perchloric acid, picric acid, hematoxylin solution, eosin Y solution, porcine gelatine,  $\beta$ -glycerolphosphate ( $\beta$ GP), ascorbic acid 2-phosphate (AA2P), dexamethasone, Triton X-100 (Triton), deoxyribonuclease (DNase), and Alizarin red S were purchased from Sigma-Aldrich (Poole, U.K.). Direct Red 80 (Sirius Red) was purchased from Fluka (Buchs, Switzerland). Chloroform, industrial methylated spirit (IMS), dichloromethane (DCM), and methanol (MeOH) were purchased from Fisher Scientific (Pittsburgh, PA). The surfactant Hypermer B246-SO-M was received as a sample from Croda (Goole, U.K.). The minimum essential  $\alpha$  medium ( $\alpha$ -MEM) was purchased from Lonza (Slough, U.K.). The Quant-iT PicoGreen (PG) dsDNA assay kit and the human fibroblastic growth factor (hFGF) were obtained from Life Technologies (Frederick, Maryland). The optimum cutting temperature tissue freezing medium (OCT-TFM) was purchased from Leica Biosystems (Newcastle, U.K.).

**2.2. Manufacturing and Characterization of the Multiscale Porous PCL Scaffolds.** Multiscale porous photocurable PCL-based scaffolds were created in three main steps: (i) synthesis of four-arm hydroxyl-terminated polycaprolactone (4PCL) and methacrylate functionalization of 4PCL (4PCLMA) to make the polymer photocurable, (ii) preparation of the emulsions made of 4PCLMA, and (iii) simultaneous 3D printing and cross-linking of 4PCLMA-based emulsions.

**2.2.1. Synthesis and Methacrylation of 4PCL.** The detailed synthesis of the polymer, 4PCLMA, has been described elsewhere.<sup>51</sup> Briefly, under nitrogen flow, pentaerythritol (0.088 mol) and  $\epsilon$ -caprolactone (0.705 mol) were added into a three-neck round-bottomed flask, and the system was heated to 160 °C using an oil bath while being mixed at 200 rpm. When the pentaerythritol was completely dissolved, the catalyst, tin(II) 2-ethyl hexanoate, was added, and the system was left overnight to form 4PCL before being removed from the oil bath and left to cool down in the ambient atmosphere.

4PCL was dissolved in 300 mL of DCM, and then TEA (0.705 mol) was added. Reagents were stirred, and a further 200 mL of DCM was added to ensure everything was dissolved. The flask was placed in an ice bath. MAAn (0.705 mol) was dissolved in 100 mL of DCM and transferred into a dropping funnel (~1 drop/s). When the MAAn was completely dispensed, the ice bath was removed, and the system was maintained at room temperature (RT) for 68 h while being mixed. It was then washed with HCl solution, and then with deionized water (dH<sub>2</sub>O) to remove TEA, MAAn, and salts formed. Almost all solvents were evaporated using a rotary evaporator. Three methanol washes were applied, and any remaining solvent was removed using a rotary evaporator. 4PCLMA was stored in the freezer (−20 °C) for further use.

**2.2.2. Characterization of 4PCL and 4PCLMA.** To confirm the structure of 4PCL and 4PCLMA and also to measure the degree of methacrylation, proton (<sup>1</sup>H) nuclear magnetic resonance (NMR) spectroscopy analysis was performed on an AVANCE III spectrometer at 400 MHz. The spectra were recorded using an 8.2 kHz acquisition window, with 64k data points in 16 transients with a 60 s recycle delay (to ensure full relaxation). Deuterated chloroform

was used as a diluent (CDCl<sub>3</sub>). Spectra were analyzed using the MestReNova software. Chemical shifts were referenced relative to CDCl<sub>3</sub> at 7.26 ppm.

The weight average molecular weight ( $M_w$ ) and number average molecular weight ( $M_n$ ) distributions of 4PCLMA were determined using a Viscotek GPCmax VE200 gel permeation chromatography (GPC) system with a differential refractive index detector (Waters 410). Tetrahydrofuran was used as the eluting solvent at a flow rate of 1 mL/min at 40 °C, and polystyrene standards were used as the calibration sample.

**2.2.3. Preparation of 4PCLMA-Based HIPES.** Throughout this study, the only polymer used was 4PCLMA, and it has been entitled as PCL in the rest of the text except Section 3.1 unless otherwise stated. PCL (0.2 g) and 10% (w/w) surfactant were added into a glass vial ( $\varnothing = 25$  mm) and heated to 40 °C to dissolve the surfactant and left for cooling. The chloroform/toluene solvent blend (40/60 (w/w), 0.3 g) was added to the PCL–surfactant mixture and mixed at 375 rpm using a magnetic stirrer for 1 min at RT. Once the homogeneous mixture was created, 2 mL of water was added dropwise for PCL HIPES (89% internal phase volume), and the emulsion was mixed for a further 5 min at 375 rpm and 5 min at 1000 rpm.

**2.2.4. Viscosity Measurements.** AR2000 (TA Instruments, New Castle, DE, USA) was used to characterize the viscosity of the PCL HIPES. Steel cone plates (40 nm, 2°) were used with a gap of 55  $\mu$ m at 25 °C. The sample (0.6 mL) was injected, and a continuous ramp step was applied with a shear between 0.01 and 10 s<sup>−1</sup> using log mode and 50 points per decade.

**2.2.5. Three-Dimensional (3D) Printing and Polymerization of PCL-Based HIPES.** A 10 × 10 × 1.4 mm<sup>3</sup> tetragonal prism was designed using Solidworks (2012) and saved as a standard tessellation language (.stl) file format. This file was imported into the Repetier host to convert .stl format to .gcode format, which is a layer by layer design of the scaffold to make it recognizable by the printer. During the conversion, the following parameters were set: layer height; 100  $\mu$ m, infill; 36% rectilinear, and speed; 13 mm/s.

The Gcode file was imported into the Bioprint software, and the PCL-based HIPE was loaded into a syringe with a 30G precision tip needle. The syringe was connected to the compressor line and placed into a three-axis dispensing control system at RT. The pressure was set to 20 psi, however, slightly adjusted throughout the process for the best results. Multiscale porous PCL scaffolds were prepared by simultaneous printing and cross-linking of the PCL-based HIPE with the help of the integrated light-emitting diode (LED) lamp of the printer (Biobot1, Allevi, Philadelphia, PA).

**2.2.6. Morphological Investigation of the Multiscale Porous PCL Scaffolds.** Scanning electron microscopy (SEM) was used to investigate the microarchitecture of the scaffolds. Samples were gold sputter-coated in 15 kV for 2.5 min to increase conductivity. A FEI Inspect F SEM (Philips/FEI XL-20 SEM, Cambridge, U.K.) was used with 10 kV power. Randomly 20 pores, 20 struts, and 50 micropores were selected, and measurements were taken. A statistical correction factor ( $2/\sqrt{3}$ ) was applied to micropore measurements to adjust the underestimation of diameter because of uneven sectioning.<sup>59</sup> The degree of interconnectivity was calculated by dividing the average window size by the average pore size ( $d/D$ ),<sup>51,60</sup> and the degree of openness was calculated by dividing the open surface area to the total surface area.<sup>34,61</sup> The window diameters of 50 micropores (426 windows in total) were measured.

**2.3. Manufacturing of the Biohybrid Scaffolds via In Vitro Generated ECM Matrix Deposition on Multiscale Porous PCL Scaffolds.** Biohybrid scaffolds, made of PCL and bone ECM, were manufactured in three main steps; (i) manufacturing of the multiscale porous PCL scaffolds as described in Section 2.2, (ii) cellularization, and (iii) decellularization of these scaffolds.

**2.3.1. Cellularization of the Multiscale Porous PCL Scaffolds with Bone Cells.** Multiscale porous PCL scaffolds were washed with 100% ethanol four times (24 h each) to remove any remaining contaminants of the surfactant, the solvent, or the uncured material. Then, they were left in 70% ethanol for 2 h and then transferred into phosphate-buffered saline (PBS) in sterile conditions; four PBS

washes were applied in 24 h.  $\alpha$ -MEM supplemented with 10% FCS, 2 mM L-glutamine, and 100 mg/mL penicillin/streptomycin was used as a basal cell culture media (BM). Scaffolds were conditioned with BM for 2 h in the incubator. Murine osteoblast/osteocyte-like cells (MLO-A5s) were defrosted into gelatine-coated T75 flasks and cultured until 90% confluence. MLO-A5s were expanded, trypsinized, counted, and centrifuged. The cell pellet was resuspended in fresh BM media (25 000 cells/20  $\mu$ m). The media in the well plate was aspirated, and 20  $\mu$ m of the cell suspension was placed on the whole surface of each scaffold homogeneously and left for 2 h in an incubator (37  $^{\circ}$ C, 5% CO<sub>2</sub>) for cell attachment. During this time, to prevent cells from drying out and keep the inside of the well humid, 4 mL of BM media was injected into the spaces between the wells. After 2 h, 2 mL of BM media was supplied into each well and incubated overnight. On the following day, scaffolds were transferred into a fresh well plate and incubated with supplemented media (SM) consisting of BM with 50  $\mu$ g/mL AA2P and 5 mM  $\beta$ GP. Cell culture media was changed every 2–3 days.

**2.3.2. Decellularization of the Multiscale Porous PCL Scaffolds Populated with Bone Cells.** Three different decellularization methods were used for devitalization of multiscale porous PCL scaffolds cultured with MLO-A5s: freezing and thawing (ft), Triton and ammonia (ta), and DNase. Four different combinations of these protocols were tested: (i) ft only, (ii) ft + ta, (iii) ft + DNase, and (iv) ft + ta + DNase, and they were compared in terms of their efficiency of DNA removal. Before applying each decellularization protocol, culture media was removed, and scaffolds were washed twice with PBS. Each method is described in the following section. At the end of the application of a decellularization method, scaffolds were washed with warm (37  $^{\circ}$ C) PBS three times to remove the cellular component. Combined protocols were applied by following the individual protocols in order.

The method of ft is categorized as mechanical decellularization, and it is applied by alternating the temperature between freezing temperatures and biological temperatures. The ft technique leads to lysis of cells with the help of intracellular ice crystals. Although this technique maintains ECM properties, its usage as a single-step method has been found to be inefficient based on DNA removal.<sup>62</sup> Herein, we applied consecutive three freeze–thaw cycles. For one freeze–thaw cycle, scaffolds were left at  $-80$   $^{\circ}$ C for 15 min and transferred into a 37  $^{\circ}$ C water bath for 30 min.

Triton is a nonionic detergent and used as a chemical decellularization agent, it disrupts lipid–lipid and lipid–protein interactions, and it is less damaging to the ECM structure in comparison with ionic detergents such as sodium dodecyl sulfate. Triton is commonly used with ammonium hydroxide (triton + ammonium hydroxide: ta), which is a base, and it also solubilizes the cell membrane and nuclear components.<sup>63</sup> Scaffolds were incubated in a 1 mL mixture of Triton (0.5%) and ammonium hydroxide (20 mM in PBS) for 10 min at 37  $^{\circ}$ C, and the solution was removed afterward.

DNase is an enzymatic decellularization agent, used for breaking down of DNA fragments and removal of the nucleotide lysis of the cell membrane with another complementary method. There are no reported adverse effects of DNase on ECM.<sup>64–66</sup> Scaffolds were incubated in 1 mL of the DNase solution (0.2 mg/mL) in an incubator for an hour.

**2.4. Cellularization of the Biohybrid Scaffolds with Mesenchymal Progenitors.** Multiscale porous PCL-only scaffolds and biohybrid scaffolds were seeded with hES-MPs (Cellartis, Sweden) for testing their biological performance. hES-MPs were defrosted into gelatine-coated T75 flasks and cultured until 90% confluence with BM. During the expansion of cells, BM was supplemented with hFGF at 4 ng/mL to stop differentiation of cells to other cell types. After the expansion of cells, they were trypsinized, counted, and centrifuged. The cell pellet was resuspended in fresh media (25 000 cells/20  $\mu$ m). The media in the 24-well plate was aspirated, and 20  $\mu$ m of the cell suspension was placed on the whole surface of each scaffold homogeneously and left for 2 h in an incubator (37  $^{\circ}$ C, 5% CO<sub>2</sub>) for cell attachment. During this time, to prevent cells from drying out and keep the inside of the well humid, 4 mL of

BM media was injected into the spaces between the wells. After 2 h, 2 mL of BM media was supplied into each well and incubated overnight. On the following day, scaffolds were transferred into the fresh well plate and incubated with osteogenic media (OM) consisting of SM with 100 nM dexamethasone. Cell culture media was changed every 2–3 days.

**2.5. Biological Characterization of PCL-Only and Biohybrid Scaffolds.**  
**2.5.1. Cell Viability Assay.** Resazurin reduction (RR) assay was applied to measure the cellular metabolic activity and estimate the cell viability on scaffolds. Resazurin solution (non-fluorescent, blue) is reduced by the cells and forms resorufin (fluorescent, pink), which is detectable by a fluorescence plate reader. Resazurin stock solution (in dH<sub>2</sub>O, 1 mM) was diluted to 100  $\mu$ M in culture media to make the resazurin working solution. Resazurin working solution (1 mL) was added into each well, and the scaffolds were transferred into a fresh well plate using sterile forceps. The well plates were protected from light and incubated for 4 h at 37  $^{\circ}$ C. From each scaffold, triplicate samples of 200  $\mu$ L of the reduced solution were added to a 96-well plate. This was measured three times using a spectrofluorometer (FLX800, BioTek Instruments, Inc.) at an excitation wavelength of 540 nm and an emission wavelength of 630 nm. RR assay was performed at days 1, 7, 14, 21, and 28 of culture for both MLO-A5s and hES-MPs using a fresh scaffold for each time point.

**2.5.2. Measuring DNA Content.** To find the cell seeding efficiencies of MLO-A5s and hES-MPs and to measure the remaining DNA content following the decellularization of the scaffolds, a QuantiT PicoGreen dsDNA assay kit was used. Scaffolds were washed with PBS three times, and 500  $\mu$ L of cell digestion buffer was added and incubated for 30 min. The three freeze–thaw cycles were applied, and scaffolds were vortexed for 15 s. Scaffolds were removed, and the remaining buffer was mixed homogeneously. The sample and the PicoGreen working solution were transferred into a 96-well plate (1:1) as triplicates. The plate was covered with an aluminum foil and incubated at RT for 10 min with gentle shaking. The resulting solution was read by using a spectrofluorometer at an excitation wavelength of 485 nm and an emission wavelength of 528 nm.

**2.5.3. Measuring ECM Deposition.** Alizarin red (AR) and Sirius red (SR) staining was conducted to measure calcium and collagen deposition, respectively. Culture media was removed, and scaffolds were washed with PBS. Scaffolds were transferred into 1 mL of 3.7% FA and left for 2 h at RT. FA was removed, and scaffolds were washed twice with dH<sub>2</sub>O. AR powder was dissolved in dH<sub>2</sub>O at 1% (w/v) in a water bath and filtered to remove particles to make Alizarin red solution (ARS). SR powder was dissolved in saturated picric acid (1% (w/v)) to form Sirius red solution (SRS) and filtered to ensure no particles remained. Scaffolds were submerged in 1 mL of SRS or ARS and left for 1 h. The solution was removed, and scaffolds were washed every 5 min with dH<sub>2</sub>O while being mixed until the water remains clear. Scaffolds were submerged with a known volume of 5% perchloric acid or 0.2 M NaOH/MeOH (1:1) to destain the AR and SR, respectively, for 30 min with gentle orbital shaking. Destain solutions (150  $\mu$ L) in triplicates were transferred into a clear 96-well plate and read at an absorbance of 405 nm.

**2.5.4. SEM of Biological Samples.** Scaffolds were washed three times with PBS after removing culture media and fixed in 2.5% (in PBS) glutaraldehyde at RT for 1 h to preserve the cell structure. They were rinsed with PBS for 15 min (three times) and soaked in dH<sub>2</sub>O for 5 min. Following this, samples were subjected to serial ethanol washes to be dehydrated (35, 60, 80, 90, and 100% for 15 min for each concentration). Finally, samples were treated with drying agent HMDS/ethanol (1:1) for 1 h and 100% HMDS for 5 min before air drying. Samples were gold-coated and visualized using methods described in Section 2.2.6.

**2.5.5. Energy-Dispersive X-ray (EDX) Analysis.** Biological samples were prepared in the same way as described in Section 2.5.4 and carbon-coated. SEM microscope (FEI Inspect F50 (Philips/FEI XL-20 SEM, Cambridge, U.K.)) with an energy-dispersive analyzer was used with 10 kV power for scanning and EDX elemental mapping.

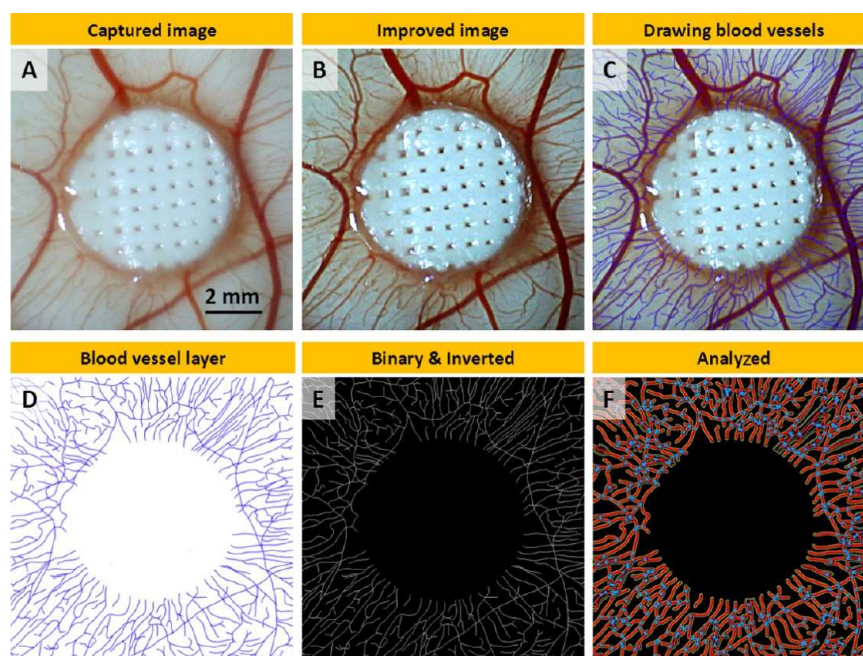


**Figure 2.** Steps of the morphometric quantification of angiogenesis: (A) macroimage as captured, (B) improved image using Photoshop (PS), (C) drawn discernable blood vessels, (D) exported blood vessel layer from PS, (E) binary and inverted images in ImageJ, (F) analyzed image using Angiotool.

**2.5.6. Ex Ovo CAM Assay.** Fertilized eggs (Henry Stewart Co. Ltd., U.K.) were cracked, and embryos were transferred into weighing boats inserted inside the Petri dishes at embryonic development day (EDD) 3. The *ex ovo* chick embryos were cultured in an incubator at 38 °C from EDD 3 to EDD 8 without any further modification. At EDD 8, PCL-only scaffolds (negative control), hybrid scaffolds, and scaffolds cultured with MLO-A5s (4 weeks) (positive control) were cut by using a sterile punch ( $\phi = 6$  mm) and placed on CAM and incubated. At EDD 14, digital images were taken, and embryos were sacrificed by cutting their arteries. Scaffolds were isolated with a 1 cm CAM margin for histological assessment.

**2.5.7. Morphometric Quantification of the Angiogenesis.** At EDD 14, the macroimages of the scaffolds on CAM were taken with a digital microscope (Figure 2A). Four digital images from each group were quantified using a modified version of a well-established method.<sup>60,61,67</sup> A 10 mm  $\times$  10 mm region was cropped in each image. To improve the discernability of the blood vessels, the following parameters were set to all images in Adobe Photoshop (PS) CS6; brightness and contrast;  $-50/10$ , unsharp;  $50/10/0$ , smart sharpen;  $100/5$  with Gaussian blur and reduced noise;  $5/0/0/50$  (Figure 2B). A new layer was created in PS, and all discernable vessels were drawn digitally using a Wacom Intuos Pro Medium Tablet with a 2 pixels size-hard round brush (Figure 2C).

The layer created for the drawing of blood vessels was exported from PS and imported into ImageJ (Figure 2D). The image was converted to binary, inverted, and saved (Figure 2E). The number of blood vessels was calculated by counting the total count of the vessels touching the border of the scaffolds. The total vessel length and the total number of junctions were quantified using Angiotool (National Cancer Institute, MD) (Figure 2F).

**2.5.8. Haematoxylin and Eosin (H&E) Staining.** Haematoxylin and eosin (H&E) staining on polyHIPE scaffolds has been described in detail elsewhere.<sup>51</sup> Briefly, scaffolds isolated from CAM were washed with PBS and fixed in 3.7% FA. Scaffolds were transferred into cryomolds filled with freezing media and frozen. Sections with 5–8  $\mu$ m thickness were sliced on glass slides using the cryostat (Leica CM1860 UV, Milton Keynes, U.K.). Slides were stained with hematoxylin and eosin for 1.5 and 5 min, respectively. After washing with dH<sub>2</sub>O, slides were dehydrated in IMS and dunked into xylene.

The slides were then mounted with DPX, and the images were captured using a light microscope (Motic BA210, China).

**2.6. Statistical Analysis.** Statistical analysis was carried out using GraphPad Prism. One-way (Figure 7A, Figure 9D–F) or two-way (Figure 6B, Figure 8B) analysis of variance (ANOVA) with multiple comparisons was performed to find the statistical significance. Where relevant, *n* values are given in figure captions. Error bars indicate standard deviations in the graphs unless otherwise stated.

### 3. RESULTS AND DISCUSSION

**3.1. Synthesis and Characterization of the Photocurable PCL.** The chemical structure and <sup>1</sup>H NMR spectra of 4PCL and 4PCLMA are given in Figure 3A–C,E. The peaks of the hydroxyl ends ( $-OH$ ) are framed with the dark gray box and labeled with “a”. These peaks represent the ends that were not methacrylated. The peaks of the methacrylate group are framed with yellow boxes and labeled with “b, c, and d”. From these results, it is clear that all of the hydroxyl ends that showed up in 4PCL have been converted to methacrylate ends following the methacrylation reaction. This suggests that the 4PCLMA used in this study is 100% methacrylated. It was reported that the higher degree of methacrylation cross-links the photocurable monomers to a higher degree, and this results in a mechanically stronger material.<sup>68–70</sup> GPC results showed that the  $M_w$  and  $M_n$  values were 2069 and 1771 g/mol, respectively, and the dispersity index was calculated as 1.17 ( $M_w/M_n$ ).

PCL is a synthetic polymer that has drawn considerable attention for use in the fabrication of TE scaffolds due to having various advantages such as being cell-compatible, bioresorbable, and having an ease of processability.<sup>71</sup> Also, PCL has been approved by the Food and Drug Administration (FDA) for its use in several medical products, such as drug delivery devices and sutures.<sup>72</sup> However, there are a limited number of studies that use photocurable PCL in biomedical applications.<sup>51,73–75</sup> Photocurable polymers need to have photoreactive groups such as acrylates or methacrylates to be

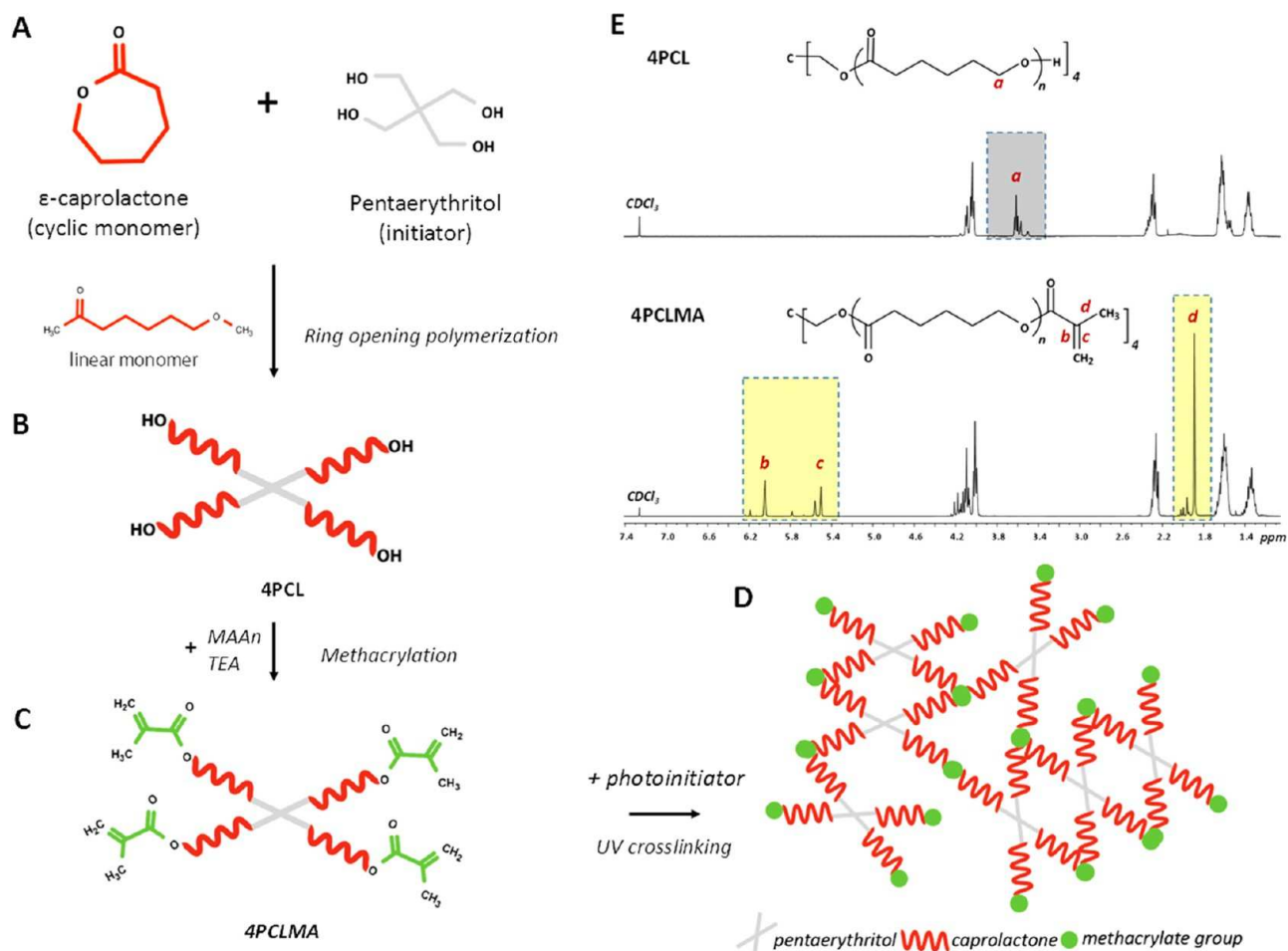


**Figure 3.** Synthesis scheme of four-arm photocurable polycaprolactone: (A, B) monomer and the initiator were used for the synthesis of hydroxyl-terminated four-arm polycaprolactone (4PCL). (B,C) 4PCL was methacrylated (4PCLMA). (D) Schematic demonstration of the photocured (UV-cross-linked) network showing a building block made of 4PCLMA. (E)  $^1\text{H NMR}$  spectrum of 4PCL, 4PCLMA, and relative assignments. Dark gray region: peaks of the hydroxyl group, light yellow regions: peaks of the methacrylate group, which only showed up after methacrylation reaction while they are absent in 4PCL.

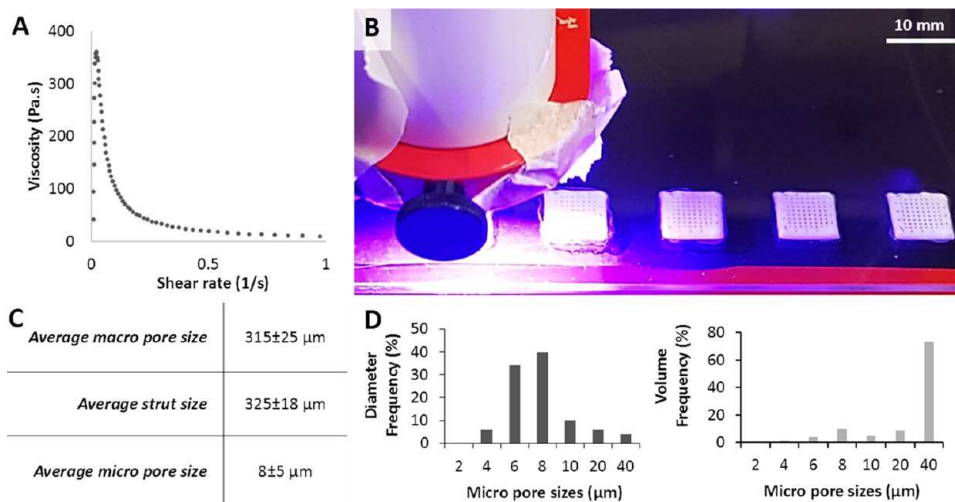


**Figure 4.** (A) Viscosity of the polycaprolactone (PCL)-based high internal phase emulsion (HIPE) prepared to be used in the printing process. (B) Three-dimensional (3D) printing and simultaneous cross-linking of PCL HIPE. (C) Morphological characterization ( $n_{\text{macro pore}} = 20$ ,  $n_{\text{strut}} = 20$ , and  $n_{\text{micropore}} = 50$ ) and (D) micropore size distribution of the scaffolds in terms of the diameter frequency and the volume frequency.

able to be cross-linked via UV and to create a polymer network in the presence of the photoinitiator (Figure 3D).<sup>74</sup> However, as commercial PCL does not contain these photoreactive

groups, photocurable PCL needs to be synthesized in-house. Photocurable polymers can be polymerized within seconds, they have higher solvent resistance over the non-cross-linked

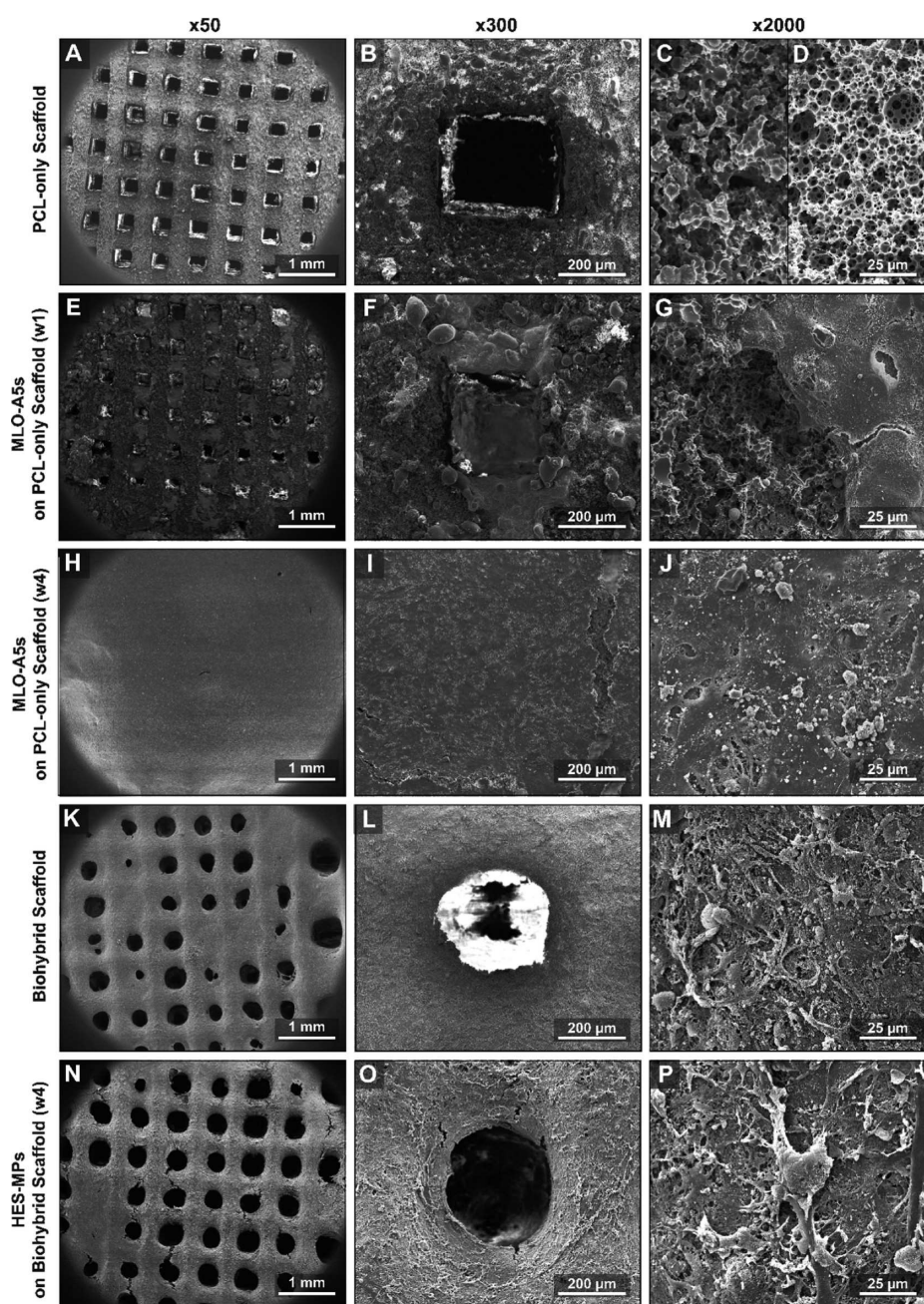


**Figure 5.** SEM micrographs of (A–D) multiscale porous PCL-only scaffolds immediately after manufacture, (E–G) after 1 week of MLO-A5 culture, (H–J) after 4 weeks of MLO-A5 culture, (K–M) after the decellularization process (biohybrid scaffold), (N–P) after 4 weeks of the culture of hES-MPs on the biohybrid scaffolds. First column macroview of the scaffold, the second column shows the single pore, and the third column shows the microsurface of the scaffold at different stages of the experiment.

polymers, and they do not need the high temperatures, which are required for thermally initiated polymerization.<sup>76</sup> Due to being processable at mild operational conditions, photocurable polymers are considered to be good candidates for use in 3D printing applications.<sup>77,78</sup>

**3.2. Fabrication of Multiscale Porous PCL Scaffolds by a Combination of Emulsion Templating and 3D Printing.** There are two main issues that should be considered in the design of emulsion inks for the 3D printing process: (i) emulsions need to have a viscosity high enough to hold the printed shape until gelation (cross-linking), (ii) emulsion-templated scaffolds need to have a pore size distribution that does not limit cell infiltration. It is essential to highlight the fact

that in w/o emulsions, emulsion viscosity is inversely proportional to the size distribution of the water droplets.<sup>79</sup> Thus, the viscosity of the emulsion should be high enough for the successful printing of the emulsion inks and low enough to enable the manufacturing of the scaffolds with pore size ranges that allow cell infiltration.

Both viscosity and pore size can be tuned by controlling the internal phase volume, the type/amount of the surfactant used, the process temperature, and mixing conditions.<sup>79–82</sup> Sears et al. reported 3D printing of acrylate-based emulsion inks, prepared by mixing up to 2500 rpm. In their study, the rheology of the inks was optimized for high accuracy printing of the emulsion to fabricate lattice design scaffolds for bone

TE, but the micropore size was not reported.<sup>30</sup> Yang et al. reported the use of mechanical shaking for the emulsification process and demonstrated the successful fabrication of 3D-printed emulsion-templated scaffolds with an average micropore size of 20  $\mu\text{m}$ .<sup>27</sup>

As relative viscosity increases with the increasing volume fraction of the dispersed phase,<sup>83,84</sup> we maximized the inner phase volume. The maximum water volume achieved was 89% where a further increase in the water volume beyond that resulted in phase separation of the emulsion at the reported process conditions. PCL-based HIPE showed shear-thinning behavior, which enables their extrusion through the nozzle with applied pressure<sup>85</sup> (Figure 4A). Throughout the printing process, no phase separation was observed in PCL-based HIPEs. Similarly, we have previously shown the stability of the photocurable PCL-based HIPEs over 5 days.<sup>51</sup>

Pore size is one of the critical features that affect the biological performance of bone TE scaffolds in terms of cell attachment, infiltration,<sup>86,87</sup> bone formation,<sup>88–90</sup> differentiation,<sup>87,91</sup> osseointegration,<sup>92,93</sup> and vascularization.<sup>89,93</sup> Recently, multiscale porous scaffolds, developed to mimic the hierarchical structure of the natural bone, have attracted great attention,<sup>94–97</sup> and multiscale porosity has been found to be more favorable for bone regeneration compared to single-scale pore designs.<sup>26,89</sup> While macropores encourage vascularization and osteointegration,<sup>96</sup> incorporation of microporosity into scaffolds has been reported to provide grooves and roughness on the surface topology of the scaffolds, which facilitate cell adhesion.<sup>89,98</sup> These also provide a larger surface area, thereby higher protein absorption.<sup>99,100</sup> The reported optimal micro- and macropore size ranges for bone TE scaffolds in the literature are conflicting, as the compositions of the scaffolds, pore shapes, mechanical properties, cell types used in the experiments, test conditions, and the duration of the experiments vary.<sup>89,101</sup> However, in general, scaffolds with macropores sized over 300  $\mu\text{m}$  and micropores sized less than 10–50  $\mu\text{m}$  have been recommended and used by many researchers for bone regeneration studies.<sup>89,96,97</sup>

In this study, the multiscale porous PCL-only scaffolds were easily fabricated by 3D printing and the simultaneous cross-linking of PCL HIPEs (Figure 4B). No post-process was required to polymerize the PCL scaffolds. The average sizes of the macropores, struts, and micropores were measured as  $315 \pm 25$ ,  $325 \pm 18$ , and  $8 \pm 5$   $\mu\text{m}$  (Figure 4C,D), respectively. Micropores of the scaffolds exhibited open-cell morphology which is characterized by the presence of windows on the walls of the pores. Average window diameter was measured as 1.6  $\mu\text{m}$ , both the degree of openness and the degree of interconnectivity of the polyHIPEs were measured as 0.2, which is in line with the reported values in the literature.

The microporous architecture of the scaffolds was found to be different at the surface of the struts compared to within the core of the scaffolds (Figure 5C,D). This is because the surface of the polyHIPE is known to be affected by the contact materials such as the mould or air, and monoliths result in different morphologies at the surface and the cross-section.<sup>52</sup> However, as the pores on the surface still exhibited an open porosity, we believe this morphological difference did not pose a limitation to our system. A similar structural difference also can be seen in the study reported by Binks et al. for 3D-printed non-photocurable PCL polyHIPE scaffolds.<sup>27</sup>

### 3.3. Generation of the Biohybrid Scaffolds and Evaluation of Their Biological Activity. 3.3.1. Bone ECM

**Deposition on the Multiscale Porous PCL Scaffolds.** MLO-A5 cells are late-stage osteoblasts (pre-osteocytes), which have been shown to mineralize in 3 days in supplemented media and to rapidly produce the bone-like matrix. We use this mouse cell line in the proof-of-concept of this study as they have been previously reported to produce mineral (in culture), which has similar characteristics to that of the native bone as measured by Fourier transformed infrared spectroscopy.<sup>102</sup>

Despite the long incubation time for cell seeding (2 h) and conditioning of the scaffolds with media, the seeding efficiency of MLO-A5s was found to be less than 15% using a DNA quantification assay (Figure 6A). This is likely because (i) the

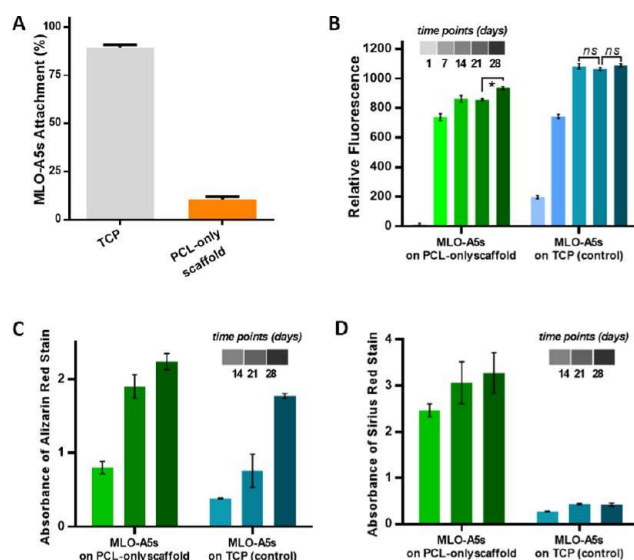


**Figure 6.** (A) Cell seeding efficiency of MLO-A5s on multiscale porous PCL-only scaffolds ( $n = 5$ ). (B) Metabolic activity ( $n = 5$ ), (C) mineral, and (D) collagen deposition of MLO-A5s on multiscale porous PCL-only scaffolds and TCP as control over 28 days ( $n = 3$ , \*:  $p < 0.05$ , ns: not significant,  $p > 0.05$ ).

macroporosity of the scaffolds caused the cell suspension to drain from the scaffolds to the tissue culture plate (TCP) and (ii) the hydrophobicity of PCL limiting the cell–surface interactions and inhibiting cell attachment. Recently, we have shown that air plasma treatment can increase cell attachment, viability, and infiltration on hydrophobic polyHIPE scaffolds.<sup>29,51</sup> However, in this study, air plasma treatment was not used to be able to show the single impact of ECM deposition on the biological activity of the scaffolds.

Although the culture began with low cell numbers on multiscale porous PCL scaffolds at day 1, the cell viability of MLO-A5s dramatically increased from day 1 to day 7 and continued to increase until day 28 (Figure 6B). Cell viability of MLO-A5s cultured on TCP increased steadily from day 1 to day 14 and then remained stable, likely due to reaching confluence in the limited two-dimensional (2D) growth area that TCP provided.

Mineral and collagen deposition of MLO-A5s cultured on multiscale porous PCL-only scaffolds showed a dramatic increase from day 14 to day 28 (Figure 6C,D). There was a progressive population of bone cells on the struts and the pores of the scaffold (Figure 5A–J). At week 4, complete coverage of the surface with cells and deposited ECM material (Figure 5H) containing mineralized nodules (Figure 5J) was observed.

**3.3.2. Decellularization of the Multiscale Porous PCL Scaffolds Populated with Bone Cells.** The fundamental aim of the decellularization process is to remove the genetic material, which may trigger an immune response<sup>103</sup> while preserving ECM components.<sup>64</sup> There are various decellularization methods described in the literature.<sup>64</sup> Depending on the target tissue, the cell line, and the scaffold design, various combinations of these methods have been performed to disintegrate the cell membrane and to remove the cellular material.<sup>104</sup> While multiple methods are combined and longer washing steps are applied for decellularization of the whole organs or tissues,<sup>64,105</sup> less harsh methods are used for decellularization of the *in vitro* generated ECM on scaffolds.<sup>2,46–50</sup>

Herein, we compared the efficiency of ft, ft + ta, ft + DNase, and ft + ta + DNase treatments in terms of DNA removal, and the remaining DNA amounts were measured as 26, 14, 5, and 4% of the total amount of initial DNA, respectively (Figure 7A). There was no significant difference found in the

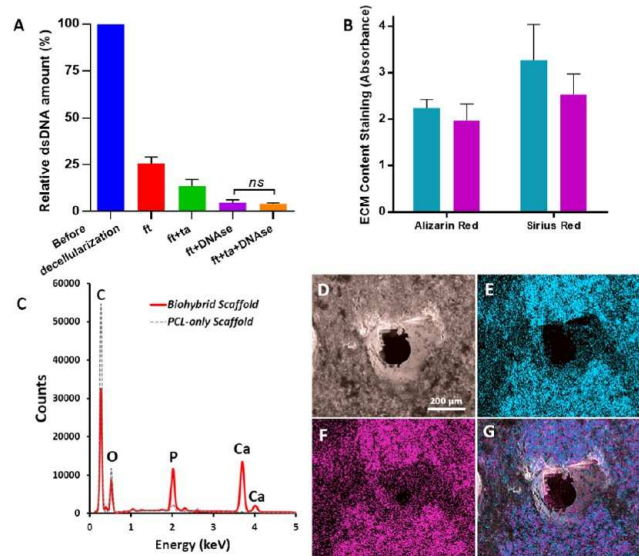


**Figure 7.** (A) Comparison of the various decellularization techniques in terms of remaining DNA content ( $n = 3$ ), (B) Calcium and collagen content of the scaffolds cultured with MLOs for 4 weeks (blue) and scaffolds that are decellularized (purple) ( $n = 3$ , ns: not significant,  $p > 0.05$ ), (C) EDX spectrum of the decellularized scaffold showing the peaks of carbon (C), phosphorus (P), calcium (Ca), and oxygen (O), (D) SEM image of the decellularized scaffold, (E–G) EDX elemental mapping of Ca (blue), P (pink), and merged mapping (Ca and P), respectively.

remaining DNA contents of the groups decellularized via ft + DNase and ft + ta + DNase. Thus, ft + DNase treatment was chosen as the decellularization method for this study due to its ability to remove DNA up to 95%.

Following the decellularization, 88 and 77% of the deposited calcium and collagen amounts were found to be preserved on biohybrid scaffolds (Figure 7B). The ft + DNase method was successful in the removal of 95% of the total DNA while preserving most of the collagen and mineral deposited onto the scaffolds. Although the macropores were covered with MLO-ASs after 4 weeks of culture, the multiple washing steps of the decellularization process seemed to disrupt the ECM layer covering the macropores and resulted in a mostly open porous structure (Figure 5K–M). EDX analysis of the biohybrid

scaffolds also showed that the remaining elemental composition consisted of mostly calcium (Ca) and phosphorus (P), the main inorganic constituents of the native bone tissue (Figure 7C–G). Some trace elements, such as sodium (Na), magnesium (Mg), silicon (Si), and sulfur (S), were also found within the deposited ECM. The small peak that corresponds to the presence of P detected on the PCL-only scaffolds is likely to come from the photoinitiator that joined the structure of the polymer during free-radical polymerization.

**3.3.3. Evaluation of the Biological Activity of the Biohybrid Scaffolds Using hES-MPs.** hES-MPs are able to differentiate into osteogenic, chondrogenic, and adipogenic cell lines. The gene expression profile of hES-MPs is similar to human mesenchymal stem cells (MSCs), but they have a higher proliferation rate.<sup>106,107</sup> In this study, they were used as a representative of osteoprogenitor cells to understand the initial steps that may occur when human osteoprogenitors encounter biohybrid scaffolds *in vivo*.

Seeding efficiencies of hES-MPs were found to be 11 and 34% on PCL-only and biohybrid scaffolds, respectively (Figure 8A). ECM deposition onto the polymeric scaffold increased

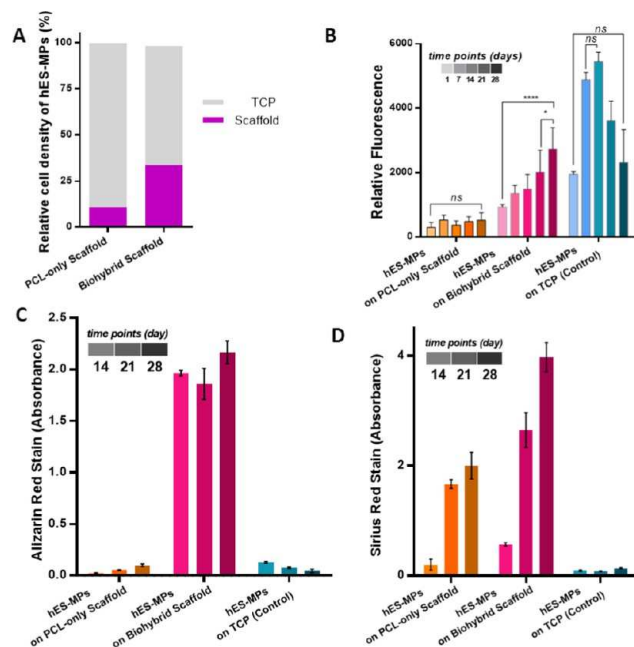


**Figure 8.** (A) Seeding efficiencies of human embryonic stem cell-derived mesenchymal progenitor cells (hES-MPs) on polycaprolactone (PCL)-only and biohybrid scaffolds ( $n = 6$ ), (B) the metabolic activity ( $n = 6$ ), (C) mineral ( $n = 3$ ), and (D) collagen deposition of hES-MPs on PCL-only, biohybrid scaffolds, and on the tissue culture plate (TCP) as a control in 28 days culture ( $n = 3$ , \*:  $p < 0.05$ , \*\*\*\*:  $p < 0.001$ , ns: not significant,  $p > 0.05$ ).

the initial cell attachment up to 3-fold compared to the PCL-only scaffold. Cell adhesion is a process that is modulated by surface receptors, integrins that can recognize ECM proteins.<sup>108</sup> Similarly, the presence of ECM proteins on the surfaces has been reported to have a positive impact on cell attachment and growth.<sup>46,109,110</sup> Also, the remaining ECM deposited on the surfaces has been reported to increase the roughness of the surfaces of the substrates, and this is likely to enhance the initial cell attachment.<sup>111</sup>

While hES-MPs cultured on PCL-only scaffolds barely survived over 28 days, the cell viability of hES-MPs cultured on

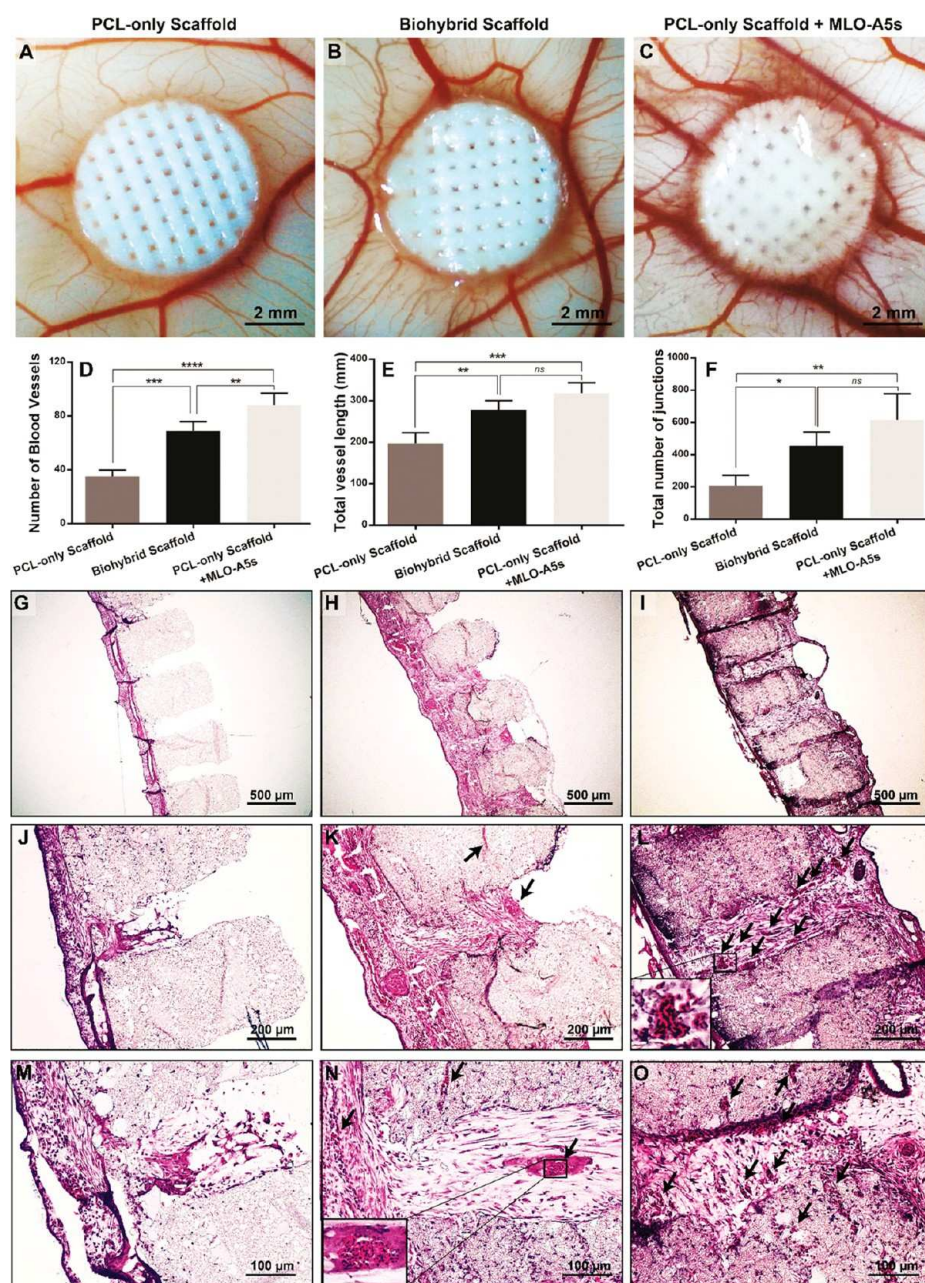


**Figure 9.** Evaluation of the angiogenic potential of polycaprolactone (PCL)-only, PCL-only populated with murine long bone osteocyte cells (MLO-A5s), and biohybrid scaffolds using chick chorioallantoic membrane (CAM) assay. (A–C) Macroimages were taken on embryonic development day 14, (D–F) quantification of the number of blood vessels, total vessel length, and the total number of junctions. ( $n = 4$ , \*:  $p < 0.05$ , \*\*:  $p < 0.01$ , \*\*\*:  $p < 0.005$ , \*\*\*\*:  $p < 0.001$ , ns: not significant,  $p > 0.05$ .) (G–O) Histological evaluation of the scaffolds isolated from CAM. (Black arrows indicate the blood vessels).

biohybrid scaffolds showed a significant increase from day 14 to day 28 (Figure 8B). The viability of hES-MPs growing on TCP increased until day 14, and cells started to detach from the surface of the TCP after that point.

Various properties, such as biochemical composition,<sup>17,112,113</sup> morphology,<sup>114</sup> and mechanical properties,<sup>115</sup> of the substrates have been shown to affect the osteogenic activities of stem cells. Similarly, in our system, the amounts of newly formed ECM, collagen, and mineral by hES-MPs on biohybrid scaffolds were dramatically higher compared with ECM deposition on PCL-only scaffolds (Figure 8C, D). Although hES-MPs cultured on both PCL-only and the biohybrid scaffolds were supplemented with OM, hES-MPs on

PCL-only scaffolds were not able to deposit a significant amount of calcium. Similar to our findings, Datta et al. previously showed that *in vitro* cell-generated ECM decoration on titanium implants stimulates the differentiation of rat marrow stromal cells even in the absence of osteogenic supplements, although this effect is shown to increase with the supplementation of osteogenic factors.<sup>46</sup> Baroncelli et al. have shown more than a 20-fold increase in the calcium deposition of MSCs on ECM-decorated substrates compared to plain ones.<sup>111</sup> Tour et al. also reported that decoration of HA scaffolds with *in vitro* generated ECM obtained from both rat osteoblasts and rat fibroblasts enhanced the osteogenic activity and reduced the inflammatory response *in vivo*.<sup>50</sup>

**3.3.4. Evaluation of the Angiogenic Activity of the Biohybrid Scaffolds Using CAM Assay.** CAM assay is a rapid (2 weeks) and a cost-effective bioassay, which has been widely accepted as an *in vivo* platform to investigate initial tissue response to biomaterials and angiogenic factors.<sup>60,116</sup> In practice, it is comparatively easier than other *in vivo* assays, most of which require several surgical procedures. The CAM assay allows direct visualization of newly formed blood vessels in the area of implantation throughout the duration of the experiment when performed *ex ovo* (shell-less).<sup>117</sup>

Angiogenesis and host tissue integration are crucial for osseointegration of bone grafts after implantation.<sup>118–120</sup> Herein, we used *ex ovo* CAM assays to evaluate: (i) initial *in vivo* response, (ii) angiogenic response, and (iii) the degree of cell and tissue integration with scaffolds.

Angiogenic effects of various cell types, including adipose-derived MSCs,<sup>67,121</sup> human dermal microvascular endothelial cells,<sup>122</sup> and fibroblasts,<sup>121,122</sup> on CAM have previously been reported. However, it has not been studied whether the cells cause the angiogenic effect or the ECM they deposit during the implantation period. In our CAM assay experiments, PCL scaffolds populated with MLO-A5 were used as the positive control and PCL-only scaffolds were used as a negative control as these should not possess any angiogenic properties.

The *ex ovo* CAM assay demonstrated that ECM deposition and the presence of MLO-A5s did not show a negative impact on the embryo survival rate, which was above 70%. Scaffolds with either ECM or live MLO-A5s significantly increased the number of blood vessels, total vessel length, and the total number of junctions in comparison to the PCL-only group (Figure 9A–F). Scaffolds cultured with MLO-A5s showed a better performance in terms of all of the three measurements mentioned above; however, only the number of blood vessels was significantly different from other groups.

At EDD 14, while isolating scaffolds, it was not possible to peel the CAM layer from the scaffold, and there was complete integration of CAM with scaffolds in all three groups (Figure 9G–O). However, while there was limited cell infiltration from CAM to the PCL-only scaffold, the ECM containing group showed higher infiltration through both macro- and micro-pores, whereas the highest infiltration was observed in the cell containing group. Additionally, blood vessels growing in the macropores were clearly detectable in the ECM and cell-loaded groups.

Pham et al. have also previously shown that *in vitro* generated ECM increased the vascularization of the constructs implanted intramuscularly in a rat animal model.<sup>2</sup> They hypothesized that it is potentially because of the contribution of the angiogenic factors that are released into the *in vitro* deposited ECM. Although future investigations are necessary to validate the composition of the ECM present here in terms of growth factors, angiogenic factors, and cytokines, our conclusions are in line with their hypothesis. Additionally, we also consider the contribution of the trace elements whose presence was verified using EDX analysis. Zhang et al. reported that Mg-, Ca-, and Si-containing ceramic scaffolds improved vascularization and bone regeneration *in vivo*.<sup>123</sup> Similarly, Mg is reported to be a vital trace element in the bone, and its role in bone regeneration and vascularization has been investigated by many other researchers.<sup>124–126</sup>

Accordingly, the findings from the quantification of both macro- and histology images support the notion that ECM deposition increased the angiogenic activity and tissue

infiltration of the PCL scaffolds. Although this response was slightly higher when the cells were maintained alive in the scaffolds, this needs to be weighed against the difficulties and limitations of implanting live cells in a clinical situation.

## 4. CONCLUSIONS

In this study, we developed biomimetic and biohybrid scaffolds for bone TE. Hierarchically porous PCL-based scaffolds were successfully fabricated by combining emulsion templating and 3D printing techniques. Following the culture of bone cells on these scaffolds for bone ECM deposition, the decellularization procedure successfully removed the 95% of the DNA, while preserving most of the collagen and mineral on the scaffolds. By testing the scaffolds for their ability to support osteoprogenitors, it was revealed that bone-derived ECM improved cell attachment, proliferation, and ECM deposition ability of hES-MPs. Bone-derived ECM also significantly improved the angiogenic activity in *ex ovo* CAM assay where the blood vessels were found to be growing through the macropores of the scaffolds on CAM. The results suggested that biohybrid scaffolds made of PCL polyHIPE and cell-generated ECM exhibit both osteogenic and angiogenic properties.

To conclude, the ECM-decorated multiscale porous scaffolds developed in this study appear to have great potential to be used as a bone graft substitute. While we used a mouse cell line in this proof-of-concept study, this technique could be easily adapted for use with the donated human MSC-derived ECM to create a product to replace the cadaveric donor bone graft or patient-specific MSCs to replace the autologous bone graft. Additionally, it will be interesting to evaluate the developed biohybrid scaffolds for their use as an *in vitro* tissue model mimicking the native bone niche.

## AUTHOR INFORMATION

### Corresponding Author

Frederik Claeysens – Department of Materials Science and Engineering, Kroto Research Institute and Department of Materials Science and Engineering, INSIGNEO Institute for In Silico Medicine, University of Sheffield, Sheffield S3 7HQ, United Kingdom; [orcid.org/0000-0002-1030-939X](https://orcid.org/0000-0002-1030-939X); Email: [f.claeysens@sheffield.ac.uk](mailto:f.claeysens@sheffield.ac.uk)

### Authors

Betül Aldemir Dikici – Department of Materials Science and Engineering, Kroto Research Institute and Department of Materials Science and Engineering, INSIGNEO Institute for In Silico Medicine, University of Sheffield, Sheffield S3 7HQ, United Kingdom; [orcid.org/0000-0002-5516-469X](https://orcid.org/0000-0002-5516-469X)

Gwendolen C. Reilly – Department of Materials Science and Engineering, INSIGNEO Institute for In Silico Medicine, University of Sheffield, Sheffield S1 3JD, United Kingdom; [orcid.org/0000-0003-1456-1071](https://orcid.org/0000-0003-1456-1071)

Complete contact information is available at: <https://pubs.acs.org/10.1021/acsami.9b23100>

### Notes

The authors declare no competing financial interest.

## ACKNOWLEDGMENTS

The authors gratefully acknowledge the Republic of Turkey—The Ministry of National Education for funding Betül Aldemir

Dikici. They also acknowledge the Engineering and Physical Sciences Research Council (Grant No. EP/I007695/1) and the Medical Research Council (Grant No. MR/L012669/1) for funding the equipment used in this study. The authors are grateful to Prof. Lynda Bonewald for her kind donation of MLO-A5 cell line. The authors would like to thank Dr. Chris Holland, Dr. Robert Owen, and Serkan Dikici for their help on viscosity measurements, the handling of hES-MPs and MLO-A5s, and CAM assay, respectively.

## REFERENCES

- (1) Campana, V.; Milano, G.; Pagano, E.; Barba, M.; Cicione, C.; Salonna, G.; Lattanzi, W.; Logroscino, G. Bone Substitutes in Orthopaedic Surgery: From Basic Science to Clinical Practice. *J. Mater. Sci. Mater. Med.* **2014**, *25*, 2445–2461.
- (2) Pham, Q. P.; Kasper, F. K.; Mistry, A. S.; Sharma, U.; Yasko, A. W.; Jansen, J. A.; Mikos, A. G. Analysis of the Osteoinductive Capacity and Angiogenicity of an in Vitro Generated Extracellular Matrix. *J. Biomed. Mater. Res., Part A* **2009**, *88A*, 295–303.
- (3) Lichte, P.; Pape, H. C.; Pufe, T.; Kobbe, P.; Fischer, H. Scaffolds for Bone Healing: Concepts, Materials and Evidence. *Injury* **2011**, *42*, 569–573.
- (4) Khan, W. S.; Rayan, F.; Dhinsa, B. S.; Marsh, D. An Osteoconductive, Osteoinductive, and Osteogenic Tissue-Engineered Product for Trauma and Orthopaedic Surgery: How Far Are We? *Stem Cells Int.* **2012**, *2012*, No. 236231.
- (5) Van Der Stok, J.; Hartholt, K. A.; Schoenmakers, D. A. L.; Arts, J. J. C. The Available Evidence on Demineralised Bone Matrix in Trauma and Orthopaedic Surgery. *Bone Jt. Res.* **2017**, *6*, 423–432.
- (6) Ranjan Dahiya, U.; Mishra, S.; Bano, S. Application of Bone Substitutes and Its Future Prospective in Regenerative Medicine. In *Biomaterial-supported Tissue Reconstruction or Regeneration*; Barbeck, M. et al., Ed.; IntechOpen, 2019.
- (7) Beebe, K. S.; Benevenia, J.; Tuy, B. E.; Depaula, C. A.; Harten, R. D.; Enneking, W. F. Effects of a New Allograft Processing Procedure on Graft Healing in a Canine Model: A Preliminary Study. *Clin. Orthop. Relat. Res.* **2009**, *467*, 273–280.
- (8) Putzer, D.; Huber, D. C.; Wurm, A.; Schmoelz, W.; Nogler, M. The Mechanical Stability of Allografts after a Cleaning Process: Comparison of Two Preparation Modes. *J. Arthroplasty* **2014**, *29*, 1642–1646.
- (9) Medical Devices Directive (MDD). <https://eur-lex.europa.eu/LexUriServ/LexUriServ.do?uri=CELEX:31993L0042:EN:HTML> (accessed Jan 31, 2020).
- (10) Medical Device Regulation (MDR). <https://eur-lex.europa.eu/legal-content/EN/TXT/PDF/?uri=CELEX:32017R0745> (accessed Jan 31, 2020).
- (11) Haugen, H. J.; Lyngstadaas, S. P.; Rossi, F.; Perale, G. Bone Grafts: Which Is the Ideal Biomaterial? *J. Clin. Periodontol.* **2019**, *46*, 92–102.
- (12) Maak, T. G.; Wylie, J. D. Medical Device Regulation: A Comparison of the United States and the European Union. *J. Am. Acad. Orthop. Surg.* **2016**, *24*, 537–543.
- (13) Hammerl, A.; Diaz Cano, C. E.; De-Juan-Pardo, E. M.; van Griensven, M.; Poh, P. S. A Growth Factor-Free Co-Culture System of Osteoblasts and Peripheral Blood Mononuclear Cells for the Evaluation of the Osteogenesis Potential of Melt-Electrowritten Polycaprolactone Scaffolds. *Int. J. Mol. Sci.* **2019**, *20*, No. 1068.
- (14) Vacanti, J. P. Beyond Transplantation: Third Annual Samuel Jason Mixer Lecture. *Arch. Surg.* **1988**, *123*, 545–549.
- (15) Langer, R.; Vacanti, J. P. Tissue Engineering. *Science* **1993**, *260*, 920–926.
- (16) Vacanti, C. A. The History of Tissue Engineering. *J. Cell. Mol. Med.* **2006**, *10*, 569–576.
- (17) Deng, Y.; Yang, W. Z.; Shi, D.; Wu, M.; Xiong, X. L.; Chen, Z. G.; Wei, S. C. Bioinspired and Osteopromotive Polydopamine Nanoparticle-Incorporated Fibrous Membranes for Robust Bone Regeneration. *NPG Asia Mater.* **2019**, *11*, No. 39.
- (18) Bhattarai, D. P.; Aguilar, L. E.; Park, C. H.; Kim, C. S. A Review on Properties of Natural and Synthetic Based Electrospun Fibrous Materials for Bone Tissue Engineering. *Membranes* **2018**, *8*, No. 62.
- (19) Taherkhani, S.; Moztafzadeh, F. Fabrication of a Poly( $\epsilon$ -Caprolactone)/Starch Nanocomposite Scaffold with a Solvent-Casting/Salt-Leaching Technique for Bone Tissue Engineering Applications. *J. Appl. Polym. Sci.* **2016**, *133*, No. 43523.
- (20) Park, H. J.; Lee, O. J.; Lee, M. C.; Moon, B. M.; Ju, H. W.; Lee, J. min.; Kim, J. H.; Kim, D. W.; Park, C. H. Fabrication of 3D Porous Silk Scaffolds by Particulate (Salt/Sucrose) Leaching for Bone Tissue Reconstruction. *Int. J. Biol. Macromol.* **2015**, *78*, 215–223.
- (21) Sultana, N.; Wang, M. PHBV/PLLA-Based Composite Scaffolds Fabricated Using an Emulsion Freezing/Freeze-Drying Technique for Bone Tissue Engineering: Surface Modification and in Vitro Biological Evaluation. *Biofabrication* **2012**, *4*, No. 015003.
- (22) Zhang, X.; Zhang, Y.; Ma, G.; Yang, D.; Nie, J. The Effect of the Prefrozen Process on Properties of a Chitosan/Hydroxyapatite/Poly(Methyl Methacrylate) Composite Prepared by Freeze Drying Method Used for Bone Tissue Engineering. *RSC Adv.* **2015**, *5*, 79679–79686.
- (23) Bose, S.; Vahabzadeh, S.; Bandyopadhyay, A. Bone Tissue Engineering Using 3D Printing. *Mater. Today* **2013**, *16*, 496–504.
- (24) Aldemir Dikici, B.; Dikici, S.; Karaman, O.; Ofiaz, H. The Effect of Zinc Oxide Doping on Mechanical and Biological Properties of 3D Printed Calcium Sulfate Based Scaffolds. *Biocybern. Biomed. Eng.* **2017**, *37*, 733–741.
- (25) Cameron, N. R. High Internal Phase Emulsion Templating as a Route to Well-Defined Porous Polymers. *Polymer* **2005**, *46*, 1439–1449.
- (26) Woodard, J. R.; Hildore, A. J.; Lan, S. K.; Park, C. J.; Morgan, A. W.; Eurell, J. A. C.; Clark, S. G.; Wheeler, M. B.; Jamison, R. D.; Wagoner Johnson, A. J. The Mechanical Properties and Osteoconductivity of Hydroxyapatite Bone Scaffolds with Multi-Scale Porosity. *Biomaterials* **2007**, *28*, 45–54.
- (27) Yang, T.; Hu, Y.; Wang, C.; Binks, B. P. Fabrication of Hierarchical Macroporous Biocompatible Scaffolds by Combining Pickering High Internal Phase Emulsion Templates with Three-Dimensional Printing. *ACS Appl. Mater. Interfaces* **2017**, *9*, 22950–22958.
- (28) Sherborne, C.; Owen, R.; Reilly, G. C.; Claeysens, F. Light-Based Additive Manufacturing of PolyHIPEs: Controlling the Surface Porosity for 3D Cell Culture Applications. *Mater. Des.* **2018**, *156*, 494–503.
- (29) Owen, R.; Sherborne, C.; Paterson, T.; Green, N. H.; Reilly, G. C.; Claeysens, F. Emulsion Templated Scaffolds with Tunable Mechanical Properties for Bone Tissue Engineering. *J. Mech. Behav. Biomed. Mater.* **2016**, *54*, 159–172.
- (30) Sears, N. A.; Dhavalikar, P. S.; Cosgriff-Hernandez, E. M. Emulsion Inks for 3D Printing of High Porosity Materials. *Macromol. Rapid Commun.* **2016**, *37*, 1369–1374.
- (31) Dhandayuthapani, B.; Yoshida, Y.; Maekawa, T.; Kumar, D. S. Polymeric Scaffolds in Tissue Engineering Application: A Review. *Int. J. Polym. Sci.* **2011**, *2011*, No. 290602.
- (32) Liu, X.; Ma, P. X. Polymeric Scaffolds for Bone Tissue Engineering. *Ann. Biomed. Eng.* **2004**, *32*, 477–486.
- (33) Cheung, H. Y.; Lau, K. T.; Lu, T. P.; Hui, D. A Critical Review on Polymer-Based Bio-Engineered Materials for Scaffold Development. *Composites, Part B* **2007**, *38*, 291–300.
- (34) Ha, T. L. B.; Quan, T. M.; Vu, D. N.; Si, D. M. Naturally Derived Biomaterials: Preparation and Application. In *Regenerative Medicine and Tissue Engineering*; Andrades, J. A., Eds.; IntechOpen, 2013.
- (35) Barua, E.; Deoghare, A. B.; Deb, P.; Lala, S. Das. Naturally Derived Biomaterials for Development of Composite Bone Scaffold: A Review. *IOP Conf. Ser.: Mater. Sci. Eng.* **2018**, *377*, No. 012013.
- (36) Jun, I. K.; Koh, Y. H.; Lee, S. H.; Kim, H. E. Novel Fabrication of a Polymer Scaffold with a Dense Bioactive Ceramic Coating Layer. *J. Mater. Sci. Mater. Med.* **2007**, *18*, 1537–1542.

- (37) Carrow, J. K.; Gaharwar, A. K. Bioinspired Polymeric Nanocomposites for Regenerative Medicine. *Macromol. Chem. Phys.* **2015**, *216*, 248–264.
- (38) Shin, H.; Jo, S.; Mikos, A. G. Modulation of Marrow Stromal Osteoblast Adhesion on Biomimetic Oligo[Poly(Ethylene Glycol) Fumarate] Hydrogels Modified with Arg-Gly-Asp Peptides and a Poly(Ethylene Glycol) Spacer. *J. Biomed. Mater. Res.* **2002**, *61*, 169–179.
- (39) Wojtowicz, A. M.; Shekaran, A.; Oest, M. E.; Dupont, K. M.; Templeman, K. L.; Hutmacher, D. W.; Guldborg, R. E.; Garcia, A. J. Coating of Biomaterial Scaffolds with the Collagen-Mimetic Peptide GFOGER for Bone Defect Repair. *Biomaterials* **2010**, *31*, 2574–2582.
- (40) Hafeman, A. E.; Li, B.; Yoshii, T.; Zienkiewicz, K.; Davidson, J. M.; Guelcher, S. A. Injectable Biodegradable Polyurethane Scaffolds with Release of Platelet-Derived Growth Factor for Tissue Repair and Regeneration. *Pharm. Res.* **2008**, *25*, 2387–2399.
- (41) Murphy, W. L.; Peters, M. C.; Kohn, D. H.; Mooney, D. J. Sustained Release of Vascular Endothelial Growth Factor from Mineralized Poly(Lactide-Co-Glycolide) Scaffolds for Tissue Engineering. *Biomaterials* **2000**, *21*, 2521–2527.
- (42) Rozario, T.; DeSimone, D. W. The Extracellular Matrix in Development and Morphogenesis: A Dynamic View. *Dev. Biol.* **2010**, *341*, 126–140.
- (43) Hersel, U.; Dahmen, C.; Kessler, H. RGD Modified Polymers: Biomaterials for Stimulated Cell Adhesion and Beyond. *Biomaterials* **2003**, *24*, 4385–4415.
- (44) Kang, Y.; Kim, S.; Khademhosseini, A.; Yang, Y. Creation of Bony Microenvironment with CaP and Cell-Derived ECM to Enhance Human Bone-Marrow MSC Behavior and Delivery of BMP-2. *Biomaterials* **2011**, *32*, 6119–6130.
- (45) Kim, H. J.; Park, J.-S. Usage of Human Mesenchymal Stem Cells in Cell-Based Therapy: Advantages and Disadvantages. *Dev. Reprod.* **2017**, *21*, 1–10.
- (46) Datta, N.; Holtorf, H. L.; Sikavitsas, V. I.; Jansen, J. A.; Mikos, A. G. Effect of Bone Extracellular Matrix Synthesized in Vitro on the Osteoblastic Differentiation of Marrow Stromal Cells. *Biomaterials* **2005**, *26*, 971–977.
- (47) Pham, Q. P.; Kurtis Kasper, F.; Scott Baggett, L.; Raphael, R. M.; Jansen, J. A.; Mikos, A. G. The Influence of an in Vitro Generated Bone-like Extracellular Matrix on Osteoblastic Gene Expression of Marrow Stromal Cells. *Biomaterials* **2008**, *29*, 2729–2739.
- (48) Thibault, R. A.; Scott Baggett, L.; Mikos, A. G.; Kasper, F. K. Osteogenic Differentiation of Mesenchymal Stem Cells on Pregelatinized Extracellular Matrix Scaffolds in the Absence of Osteogenic Cell Culture Supplements. *Tissue Eng., Part A* **2010**, *16*, 431–440.
- (49) Sadr, N.; Pippenger, B. E.; Scherberich, A.; Wendt, D.; Mantero, S.; Martin, I.; Papadimitropoulos, A. Enhancing the Biological Performance of Synthetic Polymeric Materials by Decoration with Engineered, Decellularized Extracellular Matrix. *Biomaterials* **2012**, *33*, 5085–5093.
- (50) Tour, G.; Wendel, M.; Tcacencu, I. Cell-Derived Matrix Enhances Osteogenic Properties of Hydroxyapatite. *Tissue Eng., Part A* **2011**, *17*, 127–137.
- (51) Aldemir Dikici, B.; Sherborne, C.; Reilly, G. C.; Claeysens, F. Emulsion Templated Scaffolds Manufactured from Photocurable Polycaprolactone. *Polymer* **2019**, *175*, 243–254.
- (52) Aldemir Dikici, B.; Dikici, S.; Reilly, G. C.; MacNeil, S.; Claeysens, F. A Novel Bilayer Polycaprolactone Membrane for Guided Bone Regeneration: Combining Electrospinning and Emulsion Templating. *Materials* **2019**, *12*, No. 2643.
- (53) Silverstein, M. S. PolyHIPEs: Recent Advances in Emulsion-Templated Porous Polymers. *Prog. Polym. Sci.* **2014**, *39*, 199–234.
- (54) Dikici, S.; Aldemir Dikici, B.; Bhaloo, S. I.; Balcells, M.; Edelman, E. R.; MacNeil, S.; Reilly, G. C.; Sherborne, C.; Claeysens, F. Assessment of the Angiogenic Potential of 2-Deoxy-D-Ribose Using a Novel in Vitro 3D Dynamic Model in Comparison With Established in Vitro Assays. *Front. Bioeng. Biotechnol.* **2020**, *7*, No. 451.
- (55) Ratcliffe, J. L.; Walker, M.; Eissa, A. M.; Du, S.; Przyborski, S. A.; Laslett, A. L.; Cameron, N. R. Optimized Peptide Functionalization of Thiol-Acrylate Emulsion-Templated Porous Polymers Leads to Expansion of Human Pluripotent Stem Cells in 3D Culture. *J. Polym. Sci., Part A: Polym. Chem.* **2019**, *57*, 1974–1981.
- (56) Richardson, S. A.; Rawlings, T. M.; Muter, J.; Walker, M.; Brosens, J. J.; Cameron, N. R.; Eissa, A. M. Covalent Attachment of Fibronectin onto Emulsion-Templated Porous Polymer Scaffolds Enhances Human Endometrial Stromal Cell Adhesion, Infiltration, and Function. *Macromol. Biosci.* **2019**, *19*, No. 1800351.
- (57) Akay, G.; Birch, M. A.; Bokhari, M. A. Microcellular PolyHIPE Polymer Supports Osteoblast Growth and Bone Formation in Vitro. *Biomaterials* **2004**, *25*, 3991–4000.
- (58) Wang, A.; Paterson, T.; Owen, R.; Sherborne, C.; Dugan, J.; Li, J.; Claeysens, F. Photocurable High Internal Phase Emulsions (HIPEs) Containing Hydroxyapatite for Additive Manufacture of Tissue Engineering Scaffolds with Multi-Scale Porosity. *Mater. Sci. Eng., C* **2016**, *67*, 51–58.
- (59) Barbeta, A.; Cameron, N. R. Morphology and Surface Area of Emulsion-Derived (PolyHIPE) Solid Foams Prepared with Oil-Phase Soluble Porogenic Solvents: Span 80 as Surfactant. *Macromolecules* **2004**, *37*, 3188–3201.
- (60) Dikici, S.; Mangir, N.; Claeysens, F.; Yar, M.; MacNeil, S. Exploration of 2-Deoxy-D-Ribose and 17 $\beta$ -Estradiol as Alternatives to Exogenous VEGF to Promote Angiogenesis in Tissue-Engineered Constructs. *Regener. Med.* **2019**, *14*, 179–197.
- (61) Barnhill, R. L.; Ryan, T. J. Biochemical Modulation of Angiogenesis in the Chorioallantoic Membrane of the Chick Embryo. *J. Invest. Dermatol.* **1983**, *81*, 485–488.
- (62) Lu, H.; Hoshiba, T.; Kawazoe, N.; Chen, G. Comparison of Decellularization Techniques for Preparation of Extracellular Matrix Scaffolds Derived from Three-Dimensional Cell Culture. *J. Biomed. Mater. Res., Part A* **2012**, *100A*, 2507–2516.
- (63) Bush, K.; Gertzman, A. A. Process Development and Manufacturing of Human and Animal Acellular Dermal Matrices. *Ski. Tissue Eng. Regen. Med.* **2016**, 83–108.
- (64) Gilpin, A.; Yang, Y. Decellularization Strategies for Regenerative Medicine: From Processing Techniques to Applications. *BioMed Res. Int.* **2017**, *2017*, No. 9831534.
- (65) Crapo, P. M.; Gilbert, T. W.; Badylak, S. F. An Overview of Tissue and Whole Organ Decellularization Processes. *Biomaterials* **2011**, *32*, 3233–3243.
- (66) Perea-Gil, I.; Uriarte, J. J.; Prat-Vidal, C.; Gálvez-Montón, C.; Roura, S.; Llucà-Valldeperas, A.; Soler-Botija, C.; Farré, R.; Navajas, D.; Bayes-Genis, A. In Vitro Comparative Study of Two Decellularization Protocols in Search of an Optimal Myocardial Scaffold for Recellularization. *Am. J. Transl. Res.* **2015**, *7*, 558–573.
- (67) Eke, G.; Mangir, N.; Hasirci, N.; MacNeil, S.; Hasirci, V. Development of a UV Crosslinked Biodegradable Hydrogel Containing Adipose Derived Stem Cells to Promote Vascularization for Skin Wounds and Tissue Engineering. *Biomaterials* **2017**, *129*, 188–198.
- (68) Suvarnapathaki, S.; Nguyen, M. A.; Wu, X.; Nukavarapu, S. P.; Camci-Unal, G. Synthesis and Characterization of Photocrosslinkable Hydrogels from Bovine Skin Gelatin. *RSC Adv.* **2019**, *9*, 13016–13025.
- (69) Singh, D.; Harding, A. J.; Albadawi, E.; Boissonade, F. M.; Haycock, J. W.; Claeysens, F. Additive Manufactured Biodegradable Poly(Glycerol Sebacate Methacrylate) Nerve Guidance Conduits. *Acta Biomater.* **2018**, *78*, 48–63.
- (70) Nichol, J. W.; Koshy, S. T.; Bae, H.; Hwang, C. M.; Yamanlar, S.; Khademhosseini, A. Cell-Laden Microengineered Gelatin Methacrylate Hydrogels. *Biomaterials* **2010**, *31*, 5536–5544.
- (71) Mondal, D.; Griffith, M.; Venkatraman, S. S. Polycaprolactone-Based Biomaterials for Tissue Engineering and Drug Delivery: Current Scenario and Challenges. *Int. J. Polym. Mater. Polym. Biomater.* **2016**, *65*, 255–265.

- (72) Woodruff, M. A.; Hutmacher, D. W. The Return of a Forgotten Polymer - Polycaprolactone in the 21st Century. *Prog. Polym. Sci.* **2010**, *35*, 1217–1256.
- (73) Johnson, D. W.; Langford, C. R.; Didsbury, M. P.; Lipp, B.; Przyborski, S. A.; Cameron, N. R. Fully Biodegradable and Biocompatible Emulsion Templated Polymer Scaffolds by Thiol-Acrylate Polymerization of Polycaprolactone Macromonomers. *Polym. Chem.* **2015**, *6*, 7256–7263.
- (74) He, Y.; Tuck, C. J.; Prina, E.; Kilsby, S.; Christie, S. D. R.; Edmondson, S.; Hague, R. J. M.; Rose, F. R. A. J.; Wildman, R. D. A New Photocrosslinkable Polycaprolactone-Based Ink for Three-Dimensional Inkjet Printing. *J. Biomed. Mater. Res., Part B* **2017**, *105*, 1645–1657.
- (75) Green, B. J.; Worthington, K. S.; Thompson, J. R.; Bunn, S. J.; Rethwisch, M.; Kaalberg, E. E.; Jiao, C.; Wiley, L. A.; Mullins, R. F.; Stone, E. M.; et al. Effect of Molecular Weight and Functionality on Acrylated Poly(Caprolactone) for Stereolithography and Biomedical Applications. *Biomacromolecules* **2018**, *19*, 3682–3692.
- (76) Mendes-Felipe, C.; Oliveira, J.; Etxebarria, I.; Vilas-Vilela, J. L.; Lanceros-Mendez, S. State-of-the-Art and Future Challenges of UV Curable Polymer-Based Smart Materials for Printing Technologies. *Adv. Mater. Technol.* **2019**, *4*, No. 1800618.
- (77) Matsuda, T.; Mizutani, M. Liquid Acrylate-Endcapped Biodegradable Poly( $\epsilon$ -Caprolactone-Co-Trimethylene Carbonate). II. Computer-Aided Stereolithographic Microarchitectural Surface Photoconstructs. *J. Biomed. Mater. Res.* **2002**, *62*, 395–403.
- (78) Bagheri, A.; Jin, J. Photopolymerization in 3D Printing. *ACS Appl. Polym. Mater.* **2019**, *1*, 593–611.
- (79) Ilija Anisa, A. N.; Nour, A. H. Affect of Viscosity and Droplet Diameter on Water-in-Oil (w/o) Emulsions: An Experimental Study. *World Acad. Sci., Eng. Technol.* **2010**, *62*, 691–694.
- (80) Ford, R. E.; Furmidge, C. G. L. Physico-chemical Studies on Agricultural Sprays VIII.—Viscosity and Spray Drop Size of Water-in-oil Emulsions. *J. Sci. Food Agric.* **1967**, *18*, 419–428.
- (81) Welch, C. F.; Rose, G. D.; Malotky, D.; Eckersley, S. T. Rheology of High Internal Phase Emulsions. *Langmuir* **2006**, *22*, 1544–1550.
- (82) Das, A. K.; Mukesh, D.; Swayambunathan, V.; Kotkar, D. D.; Ghosh, P. K. Concentrated Emulsions. 3. Studies on the Influence of Continuous-Phase Viscosity, Volume Fraction, Droplet Size, and Temperature on Emulsion Viscosity. *Langmuir* **1992**, *8*, 2427–2436.
- (83) Farah, M. A.; Oliveira, R. C.; Caldas, J. N.; Rajagopal, K. Viscosity of Water-in-Oil Emulsions: Variation with Temperature and Water Volume Fraction. *J. Pet. Sci. Eng.* **2005**, *48*, 169–184.
- (84) Einstein, A. Berichtigung Zu Meiner Arbeit: „Eine Neue Bestimmung Der Moleküldimensionen“. *Ann. Phys.* **1911**, *339*, 591–592.
- (85) Smith, P. T.; Basu, A.; Saha, A.; Nelson, A. Chemical Modification and Printability of Shear-Thinning Hydrogel Inks for Direct-Write 3D Printing. *Polymer* **2018**, *152*, 42–50.
- (86) Murphy, C. M.; Haugh, M. G.; O'Brien, F. J. The Effect of Mean Pore Size on Cell Attachment, Proliferation and Migration in Collagen-Glycosaminoglycan Scaffolds for Bone Tissue Engineering. *Biomaterials* **2010**, *31*, 461–466.
- (87) Zhang, Y.; Fan, W.; Ma, Z.; Wu, C.; Fang, W.; Liu, G.; Xiao, Y. The Effects of Pore Architecture in Silk Fibroin Scaffolds on the Growth and Differentiation of Mesenchymal Stem Cells Expressing BMP7. *Acta Biomater.* **2010**, *6*, 3021–3028.
- (88) Whang, K.; Elenz, D. R.; Nam, E. K.; Tsai, D. C.; Thomas, C. H.; Nuber, G. W.; Glorieux, F. H.; Travers, R.; Sprague, S. M.; Healy, K. E. Engineering Bone Regeneration with Bioabsorbable Scaffolds with Novel Microarchitecture. *Tissue Eng.* **1999**, *5*, 35–51.
- (89) Karageorgiou, V.; Kaplan, D. Porosity of 3D Biomaterial Scaffolds and Osteogenesis. *Biomaterials* **2005**, *26*, 5474–5491.
- (90) Hulbert, S. F.; Young, F. A.; Mathews, R. S.; Klawitter, J. J.; Talbert, C. D.; Stelling, F. H. Potential of Ceramic Materials as Permanently Implantable Skeletal Prostheses. *J. Biomed. Mater. Res.* **1970**, *433*.
- (91) Di Luca, A.; Ostrowska, B.; Lorenzo-Moldero, I.; Lepedda, A.; Swieszkowski, W.; Van Blitterswijk, C.; Moroni, L. Gradients in Pore Size Enhance the Osteogenic Differentiation of Human Mesenchymal Stromal Cells in Three-Dimensional Scaffolds. *Sci. Rep.* **2016**, *6*, No. 22898.
- (92) Götz, H. E.; Müller, M.; Emmel, A.; Holzwarth, U.; Erben, R. G.; Stangl, R. Effect of Surface Finish on the Osseointegration of Laser-Treated Titanium Alloy Implants. *Biomaterials* **2004**, *25*, 4057–4064.
- (93) Klenke, F. M.; Liu, Y.; Yuan, H.; Hunziker, E. B.; Siebenrock, K. A.; Hofstetter, W. Impact of Pore Size on the Vascularization and Osseointegration of Ceramic Bone Substitutes in Vivo. *J. Biomed. Mater. Res., Part A* **2008**, *85A*, 777–786.
- (94) Kim, J.; McBride, S.; Donovan, A.; Darr, A.; Magno, M. H. R.; Hollinger, J. O. Tyrosine-Derived Polycarbonate Scaffolds for Bone Regeneration in a Rabbit Radius Critical-Size Defect Model. *Biomed. Mater.* **2015**, *10*, No. 035001.
- (95) Lapczynska, H.; Galea, L.; Wüst, S.; Bohner, M.; Jerban, S.; Sweedy, A.; Doebelin, N.; van Garderen, N.; Hofmann, S.; Baroud, G.; et al. Effect of Grain Size and Microporosity on the in Vivo Behaviour of  $\beta$ -Tricalcium Phosphate Scaffolds. *Eur. Cells Mater.* **2014**, *28*, 299–319.
- (96) Lan Levengood, S. K.; Polak, S. J.; Wheeler, M. B.; Maki, A. J.; Clark, S. G.; Jamison, R. D.; Wagoner Johnson, A. J. Multiscale Osteointegration as a New Paradigm for the Design of Calcium Phosphate Scaffolds for Bone Regeneration. *Biomaterials* **2010**, *31*, 3552–3563.
- (97) Rustom, L. E.; Boudou, T.; Nemke, B. W.; Lu, Y.; Hoelzle, D. J.; Markel, M. D.; Picart, C.; Wagoner Johnson, A. J. Multiscale Porosity Directs Bone Regeneration in Biphasic Calcium Phosphate Scaffolds. *ACS Biomater. Sci. Eng.* **2017**, *3*, 2768–2778.
- (98) Ellis, M.; Jarman-Smith, M.; Chaudhuri, J. Bioreactor Systems for Tissue Engineering: A Four-Dimensional Challenge. In *Bioreactors for Tissue Engineering*; Chaudhuri, J.; Al-Rubeai, M., Eds.; Springer: Dordrecht, 2005; pp 1–18.
- (99) Yuan, H.; Kurashina, K.; De Bruijn, J. D.; Li, Y.; De Groot, K.; Zhang, X. A Preliminary Study on Osteoinduction of Two Kinds of Calcium Phosphate Ceramics. *Biomaterials* **1999**, *20*, 1799–1806.
- (100) Kim, J.; Magno, M. H. R.; Waters, H.; Doll, B. A.; McBride, S.; Alvarez, P.; Darr, A.; Vasanji, A.; Kohn, J.; Hollinger, J. O. Bone Regeneration in a Rabbit Critical-Sized Calvarial Model Using Tyrosine-Derived Polycarbonate Scaffolds. *Tissue Eng., Part A* **2012**, *18*, 1132–1139.
- (101) Bose, S.; Roy, M.; Bandyopadhyay, A. Recent Advances in Bone Tissue Engineering Scaffolds. *Trends Biotechnol.* **2012**, *30*, 546–554.
- (102) Kato, Y.; Boskey, A.; Spevak, L.; Dallas, M.; Hori, M.; Bonewald, L. F. Establishment of an Osteoid Preosteocyte-like Cell MLO-AS That Spontaneously Mineralizes in Culture. *J. Bone Miner. Res.* **2001**, *16*, 1622–1633.
- (103) Akbari-Birgani, S.; Birgani, M. T.; Ansari, H. Generation of Organs Based on Decellularized Extracellular Matrix Scaffolds. *Stem Cells Biomater. Regener. Med.* **2019**, *57*–72.
- (104) Badylak, S. F.; Freytes, D. O.; Gilbert, T. W. Reprint of: Extracellular Matrix as a Biological Scaffold Material: Structure and Function. *Acta Biomater.* **2015**, *23*, S17–S26.
- (105) Zilic, L.; Wilshaw, S. P.; Haycock, J. W. Decellularisation and Histological Characterisation of Porcine Peripheral Nerves. *Biotechnol. Bioeng.* **2016**, *113*, 2041–2053.
- (106) Karlsson, C.; Emanuelsson, K.; Wessberg, F.; Kajic, K.; Axell, M. Z.; Eriksson, P. S.; Lindahl, A.; Hyllner, J.; Strehl, R. Human Embryonic Stem Cell-Derived Mesenchymal Progenitors-Potential in Regenerative Medicine. *Stem Cell Res.* **2009**, *3*, 39–50.
- (107) De Peppo, G. M.; Svensson, S.; Lennerås, M.; Synnergren, J.; Stenberg, J.; Strehl, R.; Hyllner, J.; Thomsen, P.; Karlsson, C. Human Embryonic Mesodermal Progenitors Highly Resemble Human Mesenchymal Stem Cells and Display High Potential for Tissue Engineering Applications. *Tissue Eng., Part A* **2010**, *16*, 2161–2182.

(108) Hidalgo-Bastida, L. A.; Cartmell, S. H. Mesenchymal Stem Cells, Osteoblasts and Extracellular Matrix Proteins: Enhancing Cell Adhesion and Differentiation for Bone Tissue Engineering. *Tissue Eng., Part B Rev.* **2010**, *16*, 405–412.

(109) Shekaran, A.; Garcia, A. J. Extracellular Matrix-Mimetic Adhesive Biomaterials for Bone Repair. *J. Biomed. Mater. Res., Part A* **2011**, *96A*, 261–272.

(110) Shin, H.; Zygourakis, K.; Farach-Carson, M. C.; Yaszemski, M. J.; Mikos, A. G. Attachment, Proliferation, and Migration of Marrow Stromal Osteoblasts Cultured on Biomimetic Hydrogels Modified with an Osteopontin-Derived Peptide. *Biomaterials* **2004**, *25*, 895–906.

(111) Baroncelli, M.; Van Der Eerden, B. C. J.; Chatterji, S.; Rull Trinidad, E.; Kan, Y. Y.; Koedam, M.; Van Hengel, I. A. J.; Alves, R. D. A. M.; Fratila-Apachitei, L. E.; Demmers, J. A. A.; et al. Human Osteoblast-Derived Extracellular Matrix with High Homology to Bone Proteome Is Osteopromotive. *Tissue Eng., Part A* **2018**, *24*, 1377–1389.

(112) Chen, Y.; Lee, K.; Kawazoe, N.; Yang, Y.; Chen, G. PLGA-Collagen-ECM Hybrid Scaffolds Functionalized with Biomimetic Extracellular Matrices Secreted by Mesenchymal Stem Cells during Stepwise Osteogenesis: Co-Adipogenesis. *J. Mater. Chem. B* **2019**, *7*, 7195–7206.

(113) Deng, Y.; Wei, S.; Yang, L.; Yang, W.; Dargusch, M. S.; Chen, Z. G. A Novel Hydrogel Surface Grafted With Dual Functional Peptides for Sustaining Long-Term Self-Renewal of Human Induced Pluripotent Stem Cells and Manipulating Their Osteoblastic Maturation. *Adv. Funct. Mater.* **2018**, *28*, No. 1705546.

(114) Lyu, S.; Huang, C.; Yang, H.; Zhang, X. Electrospun Fibers as a Scaffolding Platform for Bone Tissue Repair. *J. Orthop. Res.* **2013**, *31*, 1382–1389.

(115) Yao, Q.; Cosme, J. G. L.; Xu, T.; Miszuk, J. M.; Picciani, P. H. S.; Fong, H.; Sun, H. Three Dimensional Electrospun PCL/PLA Blend Nanofibrous Scaffolds with Significantly Improved Stem Cells Osteogenic Differentiation and Cranial Bone Formation. *Biomaterials* **2017**, *115*, 115–127.

(116) Mangir, N.; Dikici, S.; Claeysens, F.; Macneil, S. Using Ex Ovo Chick Chorioallantoic Membrane (CAM) Assay to Evaluate the Biocompatibility and Angiogenic Response to Biomaterials. *ACS Biomater. Sci. Eng.* **2019**, *5*, 3190–3200.

(117) Valdes, T. I.; Kreutzer, D.; Moussy, F. The Chick Chorioallantoic Membrane as a Novel in Vivo Model for the Testing of Biomaterials. *J. Biomed. Mater. Res.* **2002**, *62*, 273–282.

(118) Santos, M. I.; Reis, R. L. Vascularization in Bone Tissue Engineering: Physiology, Current Strategies, Major Hurdles and Future Challenges. *Macromol. Biosci.* **2010**, *10*, 12–27.

(119) Frohlich, M.; Grayson, W.; Wan, L.; Marolt, D.; Drobic, M.; Vunjak-Novakovic, G. Tissue Engineered Bone Grafts: Biological Requirements, Tissue Culture and Clinical Relevance. *Curr. Stem Cell Res. Ther.* **2008**, *3*, 254–264.

(120) Wang, W.; Yeung, K. W. K. Bone Grafts and Biomaterials Substitutes for Bone Defect Repair: A Review. *Bioact. Mater.* **2017**, *2*, 224–247.

(121) Shafaat, S.; Mangir, N.; Regureos, S. R.; Chapple, C. R.; MacNeil, S. Demonstration of Improved Tissue Integration and Angiogenesis with an Elastic, Estradiol Releasing Polyurethane Material Designed for Use in Pelvic Floor Repair. *Neurourol. Urodyn.* **2018**, *37*, 716–725.

(122) Dikici, S.; Claeysens, F.; MacNeil, S. Decellularised Baby Spinach Leaves and Their Potential Use in Tissue Engineering Applications: Studying and Promoting Neovascularisation. *J. Biomater. Appl.* **2019**, *34*, 546–559.

(123) Zhang, W.; Feng, C.; Yang, G.; Li, G.; Ding, X.; Wang, S.; Dou, Y.; Zhang, Z.; Chang, J.; Wu, C.; et al. 3D-Printed Scaffolds with Synergistic Effect of Hollow-Pipe Structure and Bioactive Ions for Vascularized Bone Regeneration. *Biomaterials* **2017**, *135*, 85–95.

(124) Ma, H.; Feng, C.; Chang, J.; Wu, C. 3D-Printed Bioceramic Scaffolds: From Bone Tissue Engineering to Tumor Therapy. *Acta Biomater.* **2018**, *79*, 37–59.

(125) He, D.; Zhuang, C.; Chen, C.; Xu, S.; Yang, X.; Yao, C.; Ye, J.; Gao, C.; Gou, Z. Rational Design and Fabrication of Porous Calcium-Magnesium Silicate Constructs That Enhance Angiogenesis and Improve Orbital Implantation. *ACS Biomater. Sci. Eng.* **2016**, *2*, 1519–1527.

(126) Bandyopadhyay, A.; Bernard, S.; Xue, W.; Böse, S. Calcium Phosphate-Based Resorbable Ceramics: Influence of MgO, ZnO, and SiO<sub>2</sub> Dopants. *J. Am. Ceram. Soc.* **2006**, *89*, 2675–2688.

#### NOTE ADDED AFTER ASAP PUBLICATION

This paper was published ASAP on March 9, 2020. Because of a production error, some of the references in the list were incorrect. The corrected version was reposted on March 18, 2020.